JPL PUBLICATION 77-17

(NASA-CR-154105) MARINER VENUS MERCURY 1973 S/X-BAND EXPERIMENT (Jet Propulsion Lab.) 83 p HC A05/MF A01 CSCL 17B

N77-28356

Unclas
G3/32 39272

Mariner Venus Mercury 1973 S/X-Band Experiment

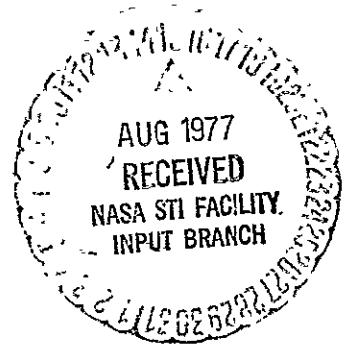

National Aeronautics and
Space Administration

Jet Propulsion Laboratory
California Institute of Technology
Pasadena, California 91103

39272 N77-28356 (NASA-CR-154105) MARINER VENUS MERCURY 1973 S/X-BAND EXPERIMENT G.S. Levy (Jet Propulsion Lab.) 1 Jul. 1977 83 p G3 D 32
Unclas

JPL PUBLICATION 77-17

Mariner Venus Mercury 1973 S/X-Band Experiment

G. S. Levy

July 1, 1977

National Aeronautics and
Space Administration

Jet Propulsion Laboratory
California Institute of Technology
Pasadena, California 91103

Prepared Under Contract No. NAS 7-100
National Aeronautics and Space Administration

PREFACE

The work described in this report was performed by the Telecommunications Science and Engineering Division of the Jet Propulsion Laboratory.

ACKNOWLEDGMENT

The S/X-band experiment described in this report was made possible by the combined sponsorship of the NASA Offices of Tracking and Data Acquisition and Aeronautics and Space Technology, which we gratefully acknowledge. W.E. Giberson's support and encouragement was crucial. D. Beauchamp and J. Dunne of the Project staff also contributed to the success of this experiment. R. Stevens, L. Randolph, J. Koukol, E. Posner, and R. Powell provided managerial and administration support. This report consists largely of excerpts of other reports; most were written by the participants in the experiment and Project. I edited these documents largely with scissors and glue bottle. Many of the documents were written by the Celestial Mechanics and Radio Science Team, led by H.T. Howard from Stanford University, and consisting of J.D. Anderson, D.L. Brunn, R. Dickinson, P.B. Esposito, G. Fjeldbo, A.J. Kliore, G.S. Levy, W.L. Martin, and C.T. Stelzried of the Jet Propulsion Laboratory, G.L. Tyler from Stanford University, and I.I. Shapiro and R.D. Reasenberg from the Massachusetts Institute of Technology. The initial breadboarding design of the XTX was conducted by R. Dickinson's Group, including R. Postal, L. Derr, B. Conroy and D. Yenche. The production of the XTX was done by the Motorola, Inc., Government Electronics Division, led by G.A. Petticrew. The implementation of the Block IV receiver was led by H. Donnelly and supported by R. Weller, C. Johns, M. Wick, H. Nishimura, E. Serhal, and S. Friedenberg. The Mu-2 ranging machine was developed by W. Martin and A. Zygielbaum, and the data interfaces were provided by J. Smith, R. Tappan, H. Baugh and D. Chaney. The dual-band ground antenna development was led by D. Bathker, with fundamental contributions by S.A. Brunstein and A.C. Ludwig and support from several others within JPL. C.T. Stelzried, B. Seidel, T. Otoshi, D.L. Brunn, and G. Wood developed the interfaces between the radio scientists, the DSN, and the Space Flight Operations Facility. The spacecraft antenna was designed by A. Brejcha and C. Smith. I would like to acknowledge the support of the staff of the NASA DSS 14 64-m station, led by C. Koscielski, and the staff of the Space Flight Operations Facility and their heroic efforts to get the system operating in a timely fashion.

ABSTRACT

The S/X-band experiment on the Mariner Venus/Mercury 1973 spacecraft constituted a unique opportunity to demonstrate the capability of an X-band downlink coherent with the normal S-band downlink. This was both a technological and scientific experiment, and the results indicated that it was successful in both cases.

Analysis of the tracking data shows that the new S/X data type was capable of reducing the miss distance at the planet Mercury by 80% (post-processed data). The use of S/X electron content was demonstrated by comparison with Faraday rotation data. An X-band turnaround telemetry experiment showed the feasibility of a planetary X-band link.

In the science area, the model atmospheric environment of Venus was refined. The ionosphere of the planet was measured to a higher accuracy than before, and the value of the dual-frequency link for measuring the scale size of turbulence was demonstrated. The estimate of the scale size was increased from 100 m to above 5 km.

At the planet Mercury, the S/X data helped establish a minimum atmospheric density.

The superior conjunction data refined our knowledge of solar corona density and scintillation characteristics.

The overall block diagram of the link as well as the implementation of the spacecraft and ground station were validated. Even those areas that were troublesome in the mission were of great value in establishing an experience base for future use of X-band for a telecommunication link.

CONTENTS

I. INTRODUCTION ---------- 1-1

II. COMMUNICATIONS LINK ---------- 2-1

A. DESCRIPTION OF THE LINK ---------- 2-1

B. ELECTRON CONTENT MEASUREMENT ---------- 2-3

C. DESIGN OF THE X-BAND TRANSMITTER ---------- 2-5

D. X-BAND TRANSMITTER SYSTEM DESCRIPTION ---------- 2-6

E. PHASE CONTROL APPROACH ---------- 2-10

F. TIME DELAY CONTROL APPROACH ---------- 2-11

G. X-BAND TRANSMITTER SUPPORT EQUIPMENT ---------- 2-11

H. TELECOMMUNICATIONS DEVELOPMENT LABORATORY FLIGHT HARDWARE TESTS ---------- 2-13

I. RANGE DELAY CALIBRATIONS ---------- 2-13

J. PHASE DELAY CALIBRATIONS ---------- 2-16

K. THERMAL VACUUM TESTING ---------- 2-17

L. THE SPACECRAFT ANTENNA SYSTEM ---------- 2-18

M. DSS 14 S/X CONFIGURATION ---------- 2-19

III. MISSION OPERATIONS ---------- 3-1

A. S/X-BAND MISSION OPERATIONS ---------- 3-1

B. EXTENDED MISSION ---------- 3-8

IV. INVESTIGATION, DESCRIPTION, AND RESULTS ---------- 4-1

A. TECHNOLOGY EXPERIMENTS WITH THE X-BAND MVM SYSTEM ---------- 4-1

1. The X-Band Telemetry Experiment ---------- 4-1

2. Navigation Enhancement Experiments ---------- 4-3

B. RADIO SCIENCE RESULTS ---------- 4-16

PRECEDING PAGE BLANK NOT FILMED

C. VENUS ENCOUNTER ---------- 4-16

D. ATMOSPHERE ---------- 4-17

E. NIGHT-SIDE IONOSPHERE ---------- 4-21

F. DAY-SIDE IONOSPHERE ---------- 4-23

G. ERROR SOURCES ---------- 4-25

H. TURBULENCE OBSERVATIONS OF THE ATMOSPHERE OF THE PLANET VENUS ---------- 4-26

I. MVM'73 MERCURY ENCOUNTER ---------- 4-28

J. SOLAR CORONA MEASUREMENTS ---------- 4-31

K. SCINTILLATION MEASUREMENTS OF THE SOLAR CORONA -------- 4-31

L. OBSERVATIONS ---------- 4-32

REFERENCES ---------- 5-1

Figures

2-1. Block Diagram of MVM'73 DSS 14 S- and X-Band Radio System ---------- 2-2

2-2. Photo of XTX Flight Package ---------- 2-7

2-3. Transmitter Block Diagram and Internal Interfaces ---------- 2-8

2-4. XTX-SE Block Diagram ---------- 2-12

2-5. TDL S/X Test Configuration ---------- 2-14

2-6. MVM'73 Flight 2 RFS/Flight SXT Ranging Group Delay vs Uplink Level ---------- 2-15

2-7. MVM'73 Flight 2 RFS/Flight XTS Differential Range Delay vs Signal Level ---------- 2-15

2-8. MVM'73 Flight 2 RFS/Flight XTX Ranging Group Delay vs Temperature ---------- 2-16

2-9. XTX Temperature Transducer vs Chamber Temperature ---------- 2-17

2-10. SXA High-Gain Antenna Feed ---------- 2-19

2-11. DSN Mission Configuration MVM-73 Tracking System, DSS 14 ---------- 2-20

2-12a. NASA/JPL 64-m Ground Antenna with Tricone Feeds ---------- 2-21

2-12b. Detail of Tricone Feeds for S-, X- and K-Bands ---------- 2-21

2-13. Conceptual Reflex-Dichroic Feed System ---------- 2-22

2-14. Detail of Reflex-Dichroic RF Optics ---------- 2-23

2-15. Basic Receiver Block Diagram ---------- 2-24

2-16. Station-Spacecraft Ranging Configuration -------- 2-26

3-1. X-Band Received Signal Level ---------- 3-1

3-2. S-Band Venus Occultation Doppler Shift ---------- 3-4

3-3. Geometry of Mercury Occultation ---------- 3-6

3-4. Differential Range Delay Near Superior Conjunction ---------- 3-8

4-1. X-Band Telemetry Experiment-Probability of Error Results ---------- 4-2

4-2. S/X Dual Doppler and Faraday Polarization Data Comparisons ---------- 4-5

4-3. High-Frequency S/X Dual Doppler Noise ---------- 4-12

4-4. MVM'73 Mercury Encounter Plane Coordinate Estimates; Impact of Faraday Calibrations ------- 4-12

4-5. MVM'73 Mercury Encounter Plane Coordinate Estimates: Impact of S/X Dual Doppler Calibrations ---------- 4-13

4-6. MVM'73 Mercury Encounter Plane Coordinate Estimates: Impact of Charged-Particle Calibrations ---------- 4-14

4-7. Noise in S/X Doppler Calibration vs SEP Angle ---------- 4-14

4-8. S- and X-Band Doppler Residuals for May 27, 1974 ---------- 4-15

4-9. S- and X-Band Doppler Residuals for June 3, 1974 ---------- 4-16

4-10. S- and X-Band Doppler Residuals for June 7, 1974 ---------- 4-17

4-11. Ratio of X-Band to S-Band Doppler Residual Noise ---------- 4-18

4-12. Venus Surface Track of Mariner 10 ---------- 4-19

4-13. DSS 14 Data Venus Temperature Profiles ---------- 4-20

4-14. DSS 12 Data Venus Temperature Profiles ---------- 4-21

4-15. Venus Ingress Electron Density ---------- 4-22

4-16. Expanded View of Venus Ingress Electron Density ---------- 4-23

4-17. Electron Densities Obtained from the Day-Side Ionosphere of Venus by MV'67 and MVM'73 ---------- 4-24

4-18. Venus Ionospheric Topside Electron Density ---------- 4-24

4-19. MVM'73 Venus Turbulence Occultation Configuration ---------- 4-27

4-20. S-Band Signal Level vs Time for Occultation Entrance ---------- 4-27

4-21. Mercury Electron Density Profiles ---------- 4-29

4-22. S- and X-Band Mercury Diffraction Effects ------- 4-30

4-23. S/X-Band Phase Difference Scintillation Spectrum ---------- 4-33

Tables

2-1. Key Parameter Data ---------- 2-9

2-2. Differential Phase Change vs Variation in Sun Simulated Intensity ---------- 2-18

3-1. Summary of DSS Receiver Events ---------- 3-5

3-2. Spacecraft and DSS Events During Mercury Occultation ---------- 3-7

SECTION I

INTRODUCTION

Mariner Venus Mercury 1973 (MVM'73) was the first planetary spacecraft to carry a dual-frequency S/X-band transmitter system.

The spacecraft equipment included the standard NASA planetary coherent turnaround S-band transponder, augmented with an additional X-band transmitter channel. The carriers of the S- and X-band signals were phase coherent and could be derived either from the local oscillator of the spacecraft receiver (when in two-way lock with the ground) or from an onboard auxiliary oscillator. Both carriers could be modulated with a common turnaround ranging signal.

Differential doppler and range were measured at the ground station. The differential doppler was used to measure the rate of change of electron density, and the differential range was used to measure the total electron content.

The objectives of the dual-frequency experiment were both technological and scientific. The technological objective was the demonstration of the dual-frequency turnaround transponder system in an interplanetary mission. The use of this system for navigation enhancement was shown. A turnaround X-band telemetry experiment was performed to learn about the problems likely to be encountered in this frequency band when used as a communications link. The difficulties associated with receiving and processing a dual-frequency signal at a ground station operationally were examined.

The scientific aspects of these experiments were the responsibility of the Celestial Mechanics and Radio Science (CMRS) Team. The scientific objectives of this team were to improve the understanding of the planetary environment, the solar wind, and the solar corona by means of the data obtained from the radio links. The radio scientists used the dual-frequency measurements to obtain the total propagation path electron content and separate the effects of neutral and charged-particle atmospheres. The celestial mechanics investigators used the dual-frequency data to eliminate the effects of charged particles from the orbit determination and analysis. The scintillation of the carriers was interpreted to determine inhomogeneities in the propagation medium. Differential amplitude measurements are being analyzed to obtain a better understanding of the planetary absorption processes.

This experiment was unique in its funding. Beause of the emphasis on the use of X-band as a future telemetry link, the NASA Office of Tracking and Data Acquisition (OTDA) and the Office of Aeronautics and Space Technology (OAST) funded the development of the flight X-band transmitter. The Mariner Venus/Mercury Project funded the testing and integration of this hardware. OTDA also funded implementation of the additional receiving equipment required to perform the experiment.

SECTION II

COMMUNICATIONS LINK

A. DESCRIPTION OF THE LINK

For MVM'73 an X-band transponder was added to the regular S-band turnaround transponder. This was the natural outgrowth of several developing scientific and technological fields--one which uses the best characteristics of spacecraft radio systems for the transmission of engineering and science data while at the same time providing fundamental radiometric data for both science and navigation (Ref. 2-1). Before the MVM mission, telemetry was handled by spacecraft S-band radio systems. The signal arriving at earth was also used for occultation measurements of planetary atmospheres and ionospheres (Ref. 2-2). During the years of development of this capability, it was not possible to modify the telemetry systems. For that reason, separate scientific instruments were flown to obtain dispersive measurements of the interplanetary medium and environment of Venus (Refs. 2-3, 2-4).

A simplified block diagram of the overall system is shown in Fig. 2-1. In the normal two-way communication mode, a command- and range-modulated 2115-MHz signal is transmitted to the spacecraft for reception on its omnidirectional antenna. This antenna was used for reception throughout the mission to assure that the spacecraft could receive commands during maneuvers and roll calibrations. The S-band receiver removed the modulation and provided a phase-coherent output to drive the S- and X-band transmitters. In the absence of an uplink signal, the receiver switched on an auxiliary crystal oscillator to provide a downlink carrier. The received range code was applied to both transmitters. The modulated outputs, 20 W at S-band and 200 mW at X-band in the precise frequency ratio of 3 to 11, were separately routed to the spacecraft transmitting antenna, a 1.37-m (54-in.) fully articulated paraboloid dish.

For the MVM'73 mission, simultaneous ground reception of the S- and X-band signals was possible at only one station of the Deep Space Network (DSN)--the 64-m antenna deep space station (DSS) 14, located at Goldstone, California. A microwave optical system directs the S- and X-band signals to separate feed horns, which drive masers tuned to 8415 and 2295 MHz. System noise temperatures obtained were 21.5 K at X-band and 13.4 K at S-band.

The telemetry and tracking ground receiver is a coherent dual-frequency, phase-locked-loop system which demodulates the telemetry and range code while extracting absolute and differential Doppler information. Range code and Doppler data are fed back to the dual-channel ranging system for processing. Doppler and range outputs are available in printed and plotted form in real time. A separate wideband, open-loop receiver system was used for occultation, with bandwidth selected to accommodate the full anticipated frequency excursion of the signal during planetary encounter. These bands were recorded coherently,

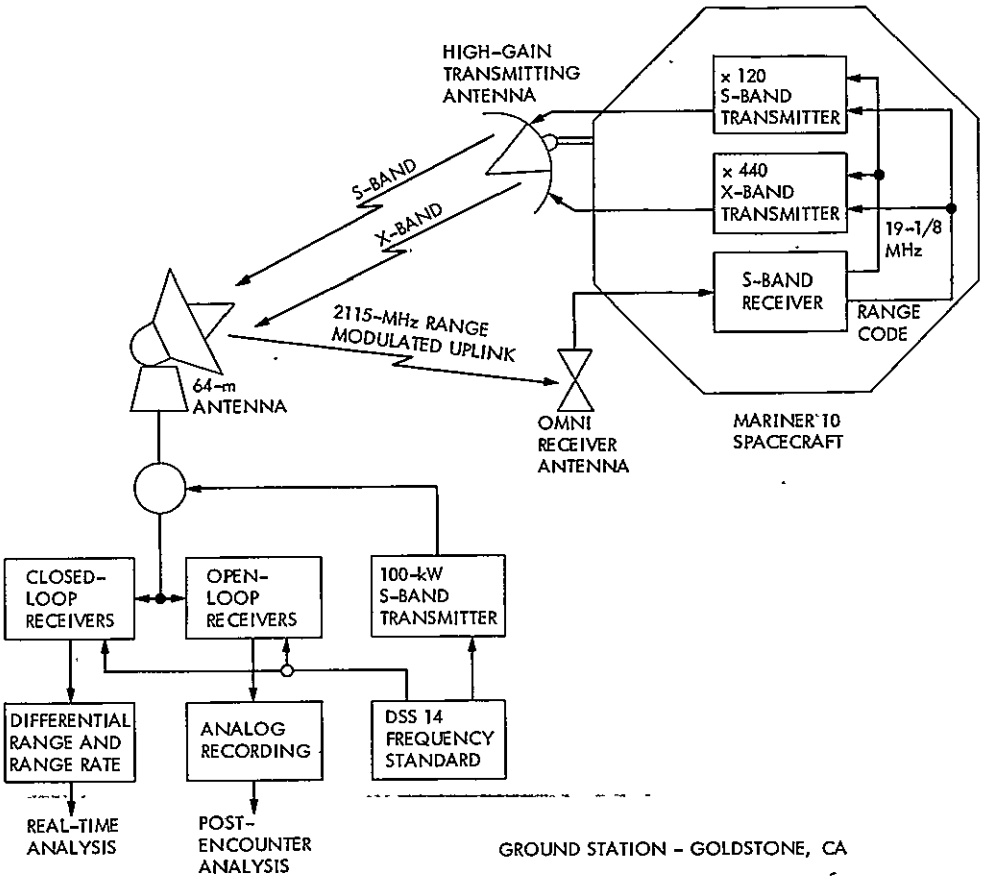

Figure 2-1. Block Diagram of MVM'73 DSS 14 S- and X-Band Radio System

along with appropriate sampling and timing signals, on analog magnetic tape recorders. The tapes were later digitized and processed by a digital simulation of the phase-locked loops. These recordings allowed the occultation to be "reflown" as many times as necessary to complete the analysis. They were of particular value at occultation emersion, where the recordings could be read backward in time, thus avoiding the problem of weak signal acquisition.

As implemented for Mariner 10, the dual-frequency system has proven fully capable of performing interplanetary columnar electron content measurements while achieving the prime goals of the Celestial Mechanics and Radio Science Teams at Venus and Mercury.

B. ELECTRON CONTENT MEASUREMENT

The major consideration for setting the specifications for the S/X experiment was the necessity for measurement of the electron content (Ref. 2-5). A modulated radio wave propagating through plasma is acted upon so that the carrier phase is advanced and the modulation, traveling at group velocity, is retarded. Thus,

$$t_p = \frac{S}{c} - \frac{40.3}{f_1^2} \int_0^S N\,dl = \text{phase transit time} \tag{1}$$

$$t_g = \frac{S}{c} + \frac{40.3}{f_1^2} \int_0^S N\,dl = \text{group transit time} \tag{2}$$

where

t_p = phase time of flight

t_g = group time of flight

S = Earth-to-spacecraft distance (m)

c = velocity of light (2.998×10^8 m/s)

f = radio wave frequency (Hz)

N = electron number density (el/m^3)

As seen from Eqs. (1) and (2), the interactive effect reduces as $1/f^2$; thus using two sufficiently separated frequencies permits very accurate measurements of plasma effects by differencing the two measurements. For a differential measurement, we have

$$\Delta t_p = -\frac{40.3}{c}\left(\frac{1}{f_1^2} - \frac{1}{f_2^2}\right)\int_0^S N\,dl\ (s) \tag{3}$$

$$\Delta t_G = \frac{40.3}{c}\left(\frac{1}{f_1^2} - \frac{1}{f_2^2}\right)\int_0^S N\,dl\ (s) \tag{4}$$

Letting $I \equiv \int_0^S N dl$ and observing that the phase delay for n cycles of S-band carrier frequency (f_1) is

$$t_n = \frac{n}{f_1}$$

we have

$$I = \frac{nc}{40.3\, f_1 \left(\frac{1}{f_1^2} - \frac{1}{f_2^2}\right)} \text{ (el/m}^2\text{)} \qquad (5)$$

Also, the modulation time delay t_m is related to the modulation phase shift ϕ (deg) by

$$t_m = \frac{\phi}{360} \frac{n}{f_1}$$

$$I = \frac{\phi c}{1.451 \times 10^4\, f_m \left(\frac{1}{f_1^2} - \frac{1}{f_2^2}\right)} \text{ (el/m}^2\text{)} \qquad (6)$$

These are the basic relationships used for evaluation of electron content. The relationships can be further simplified by evaluating for the assigned MVM'73 frequencies, where

$$f_1 = 2295.000\ 000 \text{ MHz}$$

$$f_2 = 8415.000\ 000 \text{ MHz}$$

$$f_m = 0.515{,}945 \text{ MHz}$$

These are channel center frequencies without Doppler. Using these values, we have

$$\Delta t_p = -2.36 \times 10^{-26} \int_0^S \text{Ndl (s)}$$

$$\Delta t_g = 2.36 \times 10^{-26} \int_0^S \text{Ndl (s)}$$

$$I = n(1.84 \times 10^{-16}) \text{ (el/m}^2\text{)}$$

$$I = \phi(2.28 \times 10^{-17}) \text{ (el/m}^2\text{)}$$

A differential carrier phase detection capability of 0.1 Hz would allow columnar content changes as low as 1.84×10^{14} to be measured. A 1-ns differential range detection capability would allow columnar contents as low as 4.1×10^{16} to be measured. It is seen that carrier phase measurements are approximately two orders of magnitude more sensitive than group delay measurements. This was required to detect small changes in electron content during a given tracking pass. The phase reference is lost between passes; therefore, the group delay measurements were needed to determine total electron columnar content.

For measurements of differential electron content, the stability of the phase delay through the measurement system during one pass was the basis for the specification. A maximum drift in phase of 50 cm on the spacecraft and 10 cm in the ground station for a 12-h pass was specified. Additionally, slipping of cycles by the phase-locked-loop receiver, which would cause a 360-deg discontinuity, was defined as unacceptable. In the measurement of total electron content, the difference between the absolute range at both frequencies must be known throughout the mission. The spacecraft maximum differential group delay drift of 100 cm was established for the entire mission with a calibration accuracy of 15 cm. For the ground station, where daily recalibrations could be accomplished, the specification was a maximum of 20 cm drift for a 12-h pass with an accuracy of 15 cm. A drift of 1 m produces an apparent change in electron content of approximately 1.4×10^{17} el/m^2.

C. DESIGN OF THE X-BAND TRANSMITTER

A breadboard model X-band transmitter (XTX) was constructed at JPL to demonstrate the feasibility of meeting the project requirements. The critical parameters verified were group and phase stability and dc to RF

efficiency. The breadboard model did establish the feasibility of a stripline coherent X-band exciter to be used with the standard S-band transponder. Motorola, Government Electronics Division, was then awarded a contract to design, document, fabricate, assemble, and test the X-band transmitter (Ref. 2-6). A complete breadboard and engineering model system were fabricated during the design portion of the program. A prototype (which was later to become the flight spare) and the flight unit were fabricated.

The key design parameters for the XTX were defined as

(1) Output phase shift ($\Delta\phi$) of less than 1300 deg from 0 to 55°C.

(2) Ranging time delay (ΔT) from 0 to 55°C of less than 1 ns from the 25°C reading.

(3) X-band output level of +23 ± 1 dB from 0 to 55°C.

(4) 19-MHz sidebands, at X-band output, 30 dB down.

(5) Input power of 11.5 W nominal, 12.7 W maximum, with a 25- to 50-V input voltage range.

(6) Corona allowable but with no damage. No multipacting was permissible.

(7) Maximum weight of 1.58 kg.

(8) Maximum size of 1802 cm^3.

D. X-BAND TRANSMITTER SYSTEM DESCRIPTION

Figure 2-2 is a photograph of the completed X-band transmitter. The X-band transmitter subsystem consisted of an RF switch, four frequency multiplier stages, four power amplifier stages, and a phase modulator. A block diagram of the transmitter is shown in Fig. 2-3. The input signal was at 19.125 MHz, with a nominal level of 0 dBm. The system selected on command one of two inputs, and amplified, multiplied, and phase modulated the signal to a nominal power level of 200 MW at 8415 MHz. The sequence of multiplication in the transmitter subsystem is X11 multiplier from 19.125 MHz to 210.3 MHz, quadrupler from 213.3 to 841.5 MHz, doubler from 841.5 MHz to 1683 MHz, and quintupler from 1683 MHz to 8415 MHz. There are four power amplifiers involved in the system design, as shown in the block diagram. Table 2-1 presents the performance data.

The multiplier/amplifier configuration provided the following advantages to the transmitter design and performance:

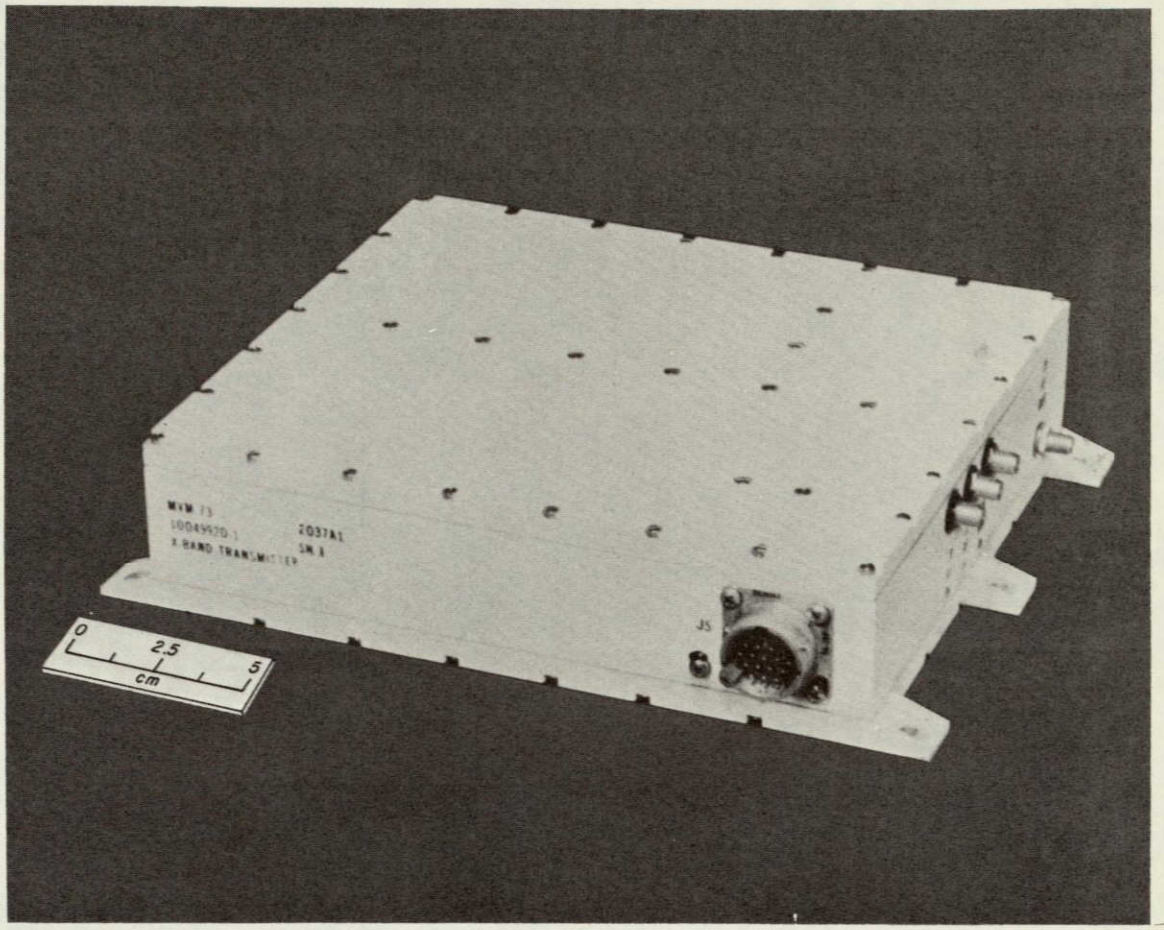

Figure 2-2. Photo of XTX Flight Package

(1) By using X11 as the first multiplier, instead of a higher-order multiplier, phase variations as a function of temperature were minimized. The X11 also minimized the filtering problem since the X11 filter could have a wider fractional bandwidth. This wider bandwidth also allowed easier phase compensation. By adequately filtering the 19.125-MHz sidebands after the X11, the filters after the modulator could have wide bandwidth and contribute a minimum of group delay variations with temperature.

(2) The phase modulator was designed at the highest practical frequency to achieve the required modulation parameters. The group delay stability requirement was more easily attained as the modulator frequency was increased because

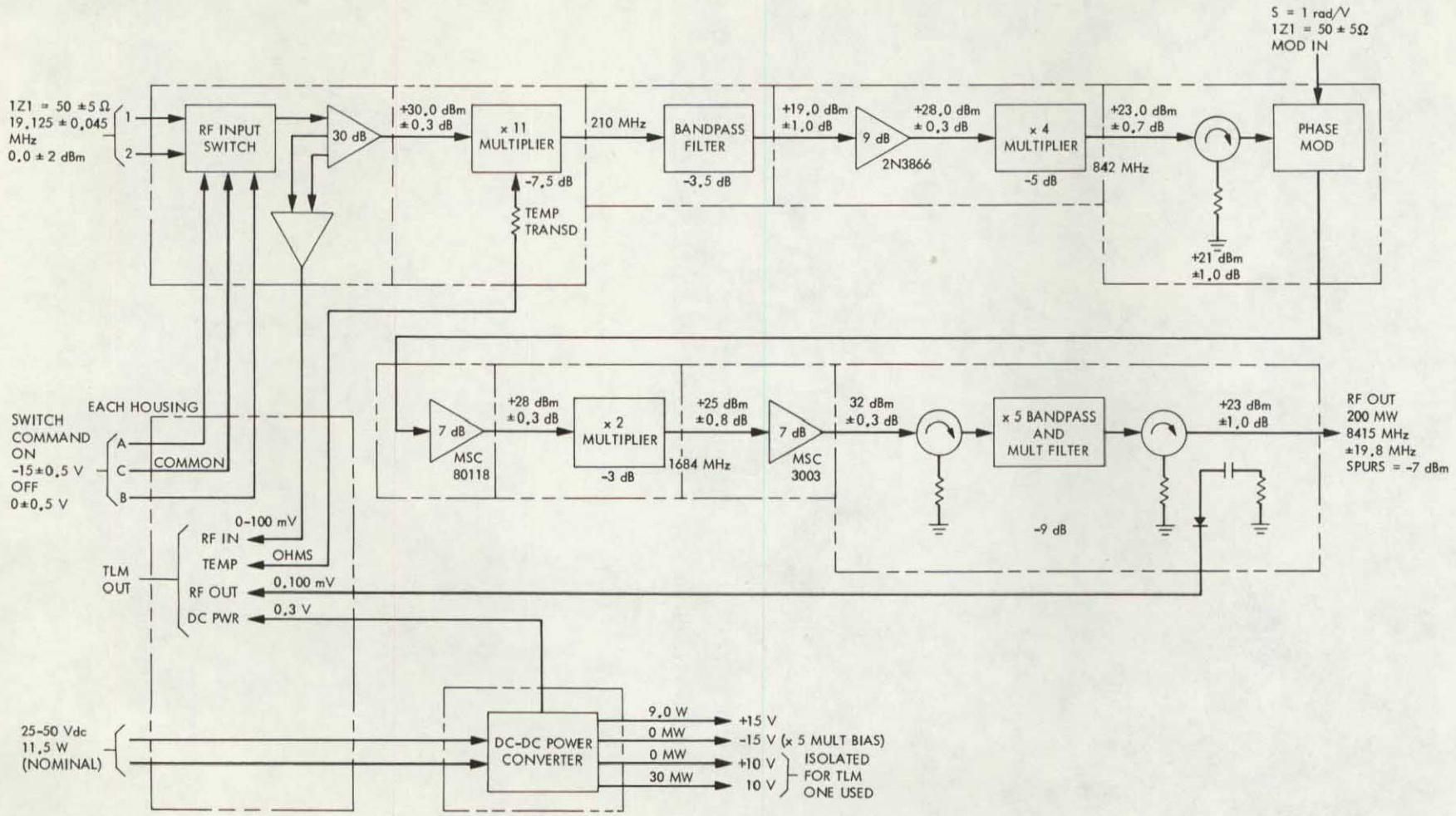

Figure 2-3. Transmitter Block Diagram and Internal Interfaces

Table 2-1. Key Parameter Data

Parameter	Specified performance	Typical data
Frequency		
Input	19 MHz ± 45 kHz	19 MHz ± 45 kHz
Output	8415 ± 19.8 MHz	8415 ± 19.8 MHz
DC input power		
Nominal	11.5 W	11.0 W
Maximum	12.7 W	12.0 W
Rf input power	0 dBM ± 2 dB	0 dBm ± 2 dB
Rf output power		
FA (0 to 55°C) + 23 ± 1 dBm		24 ± 1 dBm
TA (-20 to 75°C) + 23 ± 3 dBm		$+24\ ^{+1}_{-2}$ dBm
Carrier phase stability (0 to 55°C)	1300 deg max.	500 deg
Harmonics (related to 19-MHz input)		
2041 to 2166 MHz	-80 dBm max.	-93 dBm
All others (including -30 dB 1st 19-MHz sidebands)		-35 dB
Modulation		
Max. input level	Not specified	2 V peak
Impedance	50 ± 5 ± j5 Ω	49 ± J0
Sensitivity	1 rad/V	1.4 rad/V capability
Sens. stability		
FA (0 to 55°C)	±5%	+8%
TA (-20 to +75°C)	±7%	±15%
Linearity	2% of BSL up to 1.5 rad	2% of BSL up to 3.0 rad
Amplitude modulation (AM)		
No modulation	1%	0.5%
With modulation	2%	1.0%

Table 2-1. Key Parameter Data (Continuation 1)

Parameter	Specified performance	Typical data
Group delay stability $\left(25^{+30}_{-25}{}^{\circ}C\right)$	±1 ns	±2.5 ns
Weight	1.6 kg	1.78

of the wider bandwidth and fewer tuned circuits that passed the modulated signal.

(3) Maximum efficiency was achieved since the high-frequency, high-power multipliers were of low order.

(4) Each multiplier was preceded by a saturated amplifier to keep the drive level into the multipliers as stable as possible under temperature fluctuations. This stable drive kept the multiplier phase shift to a minimum, and minimized the phase shift for stable time delay characteristics. The saturated amplifier designs were also used as a method for meeting the ±1 dB maximum output power variation requirement with temperature (0 to 55°C).

(5) The block diagram allowed maximum mechanical flexibility in terms of the compartmentation necessary for shielding between stages. The low-frequency modules (through the phase modulator) were mounted on one side of the center web and the high-frequency modules (through the output coupler) on the other side.

E. PHASE CONTROL APPROACH

The phase shift ($\Delta\phi$) was controlled by the following techniques:

(1) The phase shift at the module level was kept to a minimum by use of wideband and phase compensation techniques.

(2) Phase shift due to drive level variations in the multipliers was kept to a minimum by operating the multiplier driving amplifiers in the saturated region, thereby keeping the amplifier outputs constant over the temperature range.

(3) The phase shift was reduced to manageable levels by controlling module and interface drive levels, and a phase control network was added to the RF switch to provide a method for controlling variations from unit to unit. The RF switch was selected for the phase control network since

a 1-deg phase shift at 19.125 MHz gave 440 deg at 8415 MHz. Both the flight unit and spare had approximately +500 deg of $\Delta\phi$ from 0 to 55°C.

F. TIME DELAY CONTROL APPROACH

The time delay (ΔT) was controlled by using wideband RF and baseband designs. The basic goal was to keep the absolute time delay small (approximately 25 ns) so that the ΔT with temperature could be kept to a minimum.

The original allotment for the X5 multiplier was ±0.4 ns, but the final design was approximately ±1.7 ns at 25^{+30}_{-25}°C.

The actual time delay measured on the engineering model unit was ±2.5 ns and ±2.0 ns on the prototype. The flight units was ±2 ns from +15 to 55°C but varied $^{+2}_{-6}$ ns from 0 to 55°C. The module or modules causing the excessive time delay from 0 to +15°C are not known.

Early in the design phase, time was spent in considering a system ΔT adjustment such as a minimum loss network with a variable phase slope with additional variability as a function of temperature. The decision was made not to implement such a device mainly because of size limitations. A system ΔT adjustment was necessary to be able to consistently meet a ±2 ns ΔT specification.

G. X-BAND TRANSMITTER SUPPORT EQUIPMENT

One of the most difficult aspects of the XTX program was the development of the appropriate support equipment (SE). The objective of this equipment was to provide the facilities necessary for complete calibration of the XTX, both in a stand-alone mode and in the spacecraft environment. The test equipment was required to calibrate instabilities in phase and group delay as a function of temperature, input voltage, transmitter drive, mode change, gain, and change in redundant components. Phase variations of 1/2 m in 12 h and delay changes of 1 m in 6 months were the desired characteristics. Signal power was to be measured to ±1% and modulation index of the X-band ranging to ±2.5%. Differential phase measurements were required between the S-band uplink and the S and X downlinks. Differential phase between the S- and X-band downlink in the one-way mode was also required.

The block diagram of this system is shown in Fig. 2-4. The SE was designed around the Hewlett Packard 8410A network analyzer, which was modified to measure S-band, X-band, and S-(3/11)X phase comparisons as well as being used for a frequency reference. The XTX SE was used in conjunction with the Radio Frequency System (RFS) SE to perform all the combined RFS-XTX system testing in the spacecraft thermal vacuum and the prelaunch tests at Cape Canaveral. The Reference Signal System supplied frequency references to the RFS and the S- and X-band phase comparators.

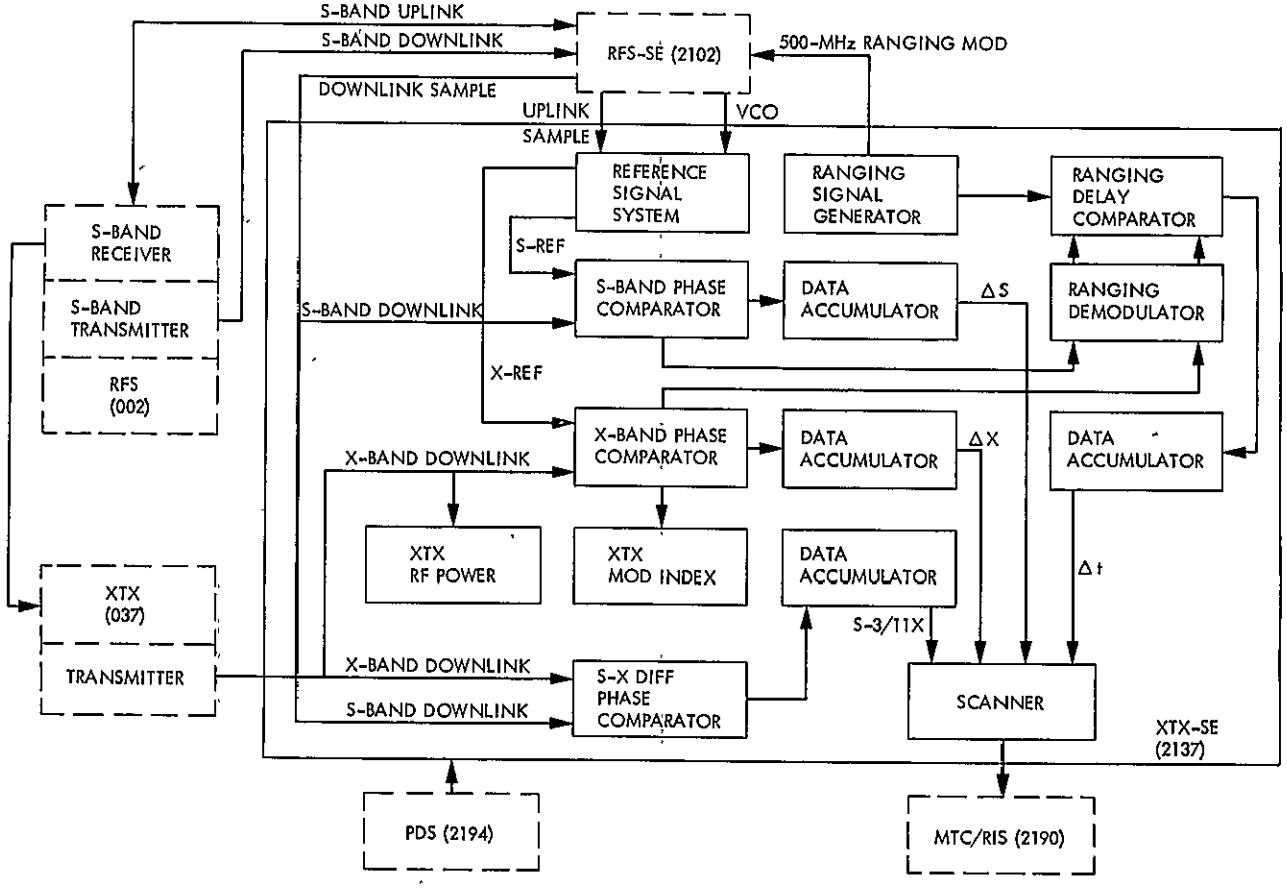

Figure 2-4. XTX-SE Block Diagram

The RFS SE then supplied the uplink to the RFS, which in turn gave a reference to the XTX. Since the reference in the S and X phase comparators was coherent with the uplink, phase shift between the three frequencies could be accurately measured. The S-X differential phase comparator compared the phase difference between the S-band downlink and the X-band downlink multiplied by 3/11. The data were accumulated locally and logged on the Mission Test Computer (MTC) (Ref. 2-7).

The XTX-SE also successfully measured X-band power and range modulation index. The range delay measurements, however, were unsatisfactory. The signal-to-noise ratio was inadequate to perform this task in an analog fashion. The decision was therefore made to make all the range delay measurements using a sequential digital ranging machine working with a DSN-type receiver-exciter system.

H. TELECOMMUNICATIONS DEVELOPMENT LABORATORY FLIGHT HARDWARE TESTS

The Telecommunications Development Laboratory (TDL) was equipped with an S-band exciter, S- and X-band receiver, and a sequential ranging machine, all of which were functionally similar to those used at the 64-m DSN station at Goldstone. A block diagram of the test configuration is shown in Fig. 2-5. The Radio Frequency System Mission Data System (MDS) and XTX were installed in a Tenney temperature control chamber, which, along with its associated operational support equipment, was located in an RF-shielded room with interconnections to the ground test equipment (Refs. 2-8, 2-9, 2-10).

I. RANGE DELAY CALIBRATIONS

Range delay calibrations at S- and X-band were performed as a function of uplink signal level, temperature, and radio operating mode. The measurements were made with a sequential ranging machine of a type similar to the DSS 14 Mu-2 ranging subsystem. Prior to performing these calibrations, comparative measurements were made using the Mu ranging machine and the TDL ranging test set. Delay measurements of the proof test model (PTM) RFS/engineering model (EM) XTX were found to agree within <2 ns when either machine was used. Also, the transponder delay was within 3 ns of a measurement made 4 months previously. Based on this data plus other measurements made on Mariner Mars 1971 (MM'71) flight equipment and delay standards, the measurement accuracy is estimated to be better than ±10 ns. The delay data is for RFS and XTX subsystems only and does not include antenna cables.

Delay as a function of uplink signal level is shown in Fig. 2-6. This curve is very similar in shape and magnitude to the previously tested units.

Differential delay versus level is shown in Fig. 2-7. Approximately 5 to 7 ns change was observed.

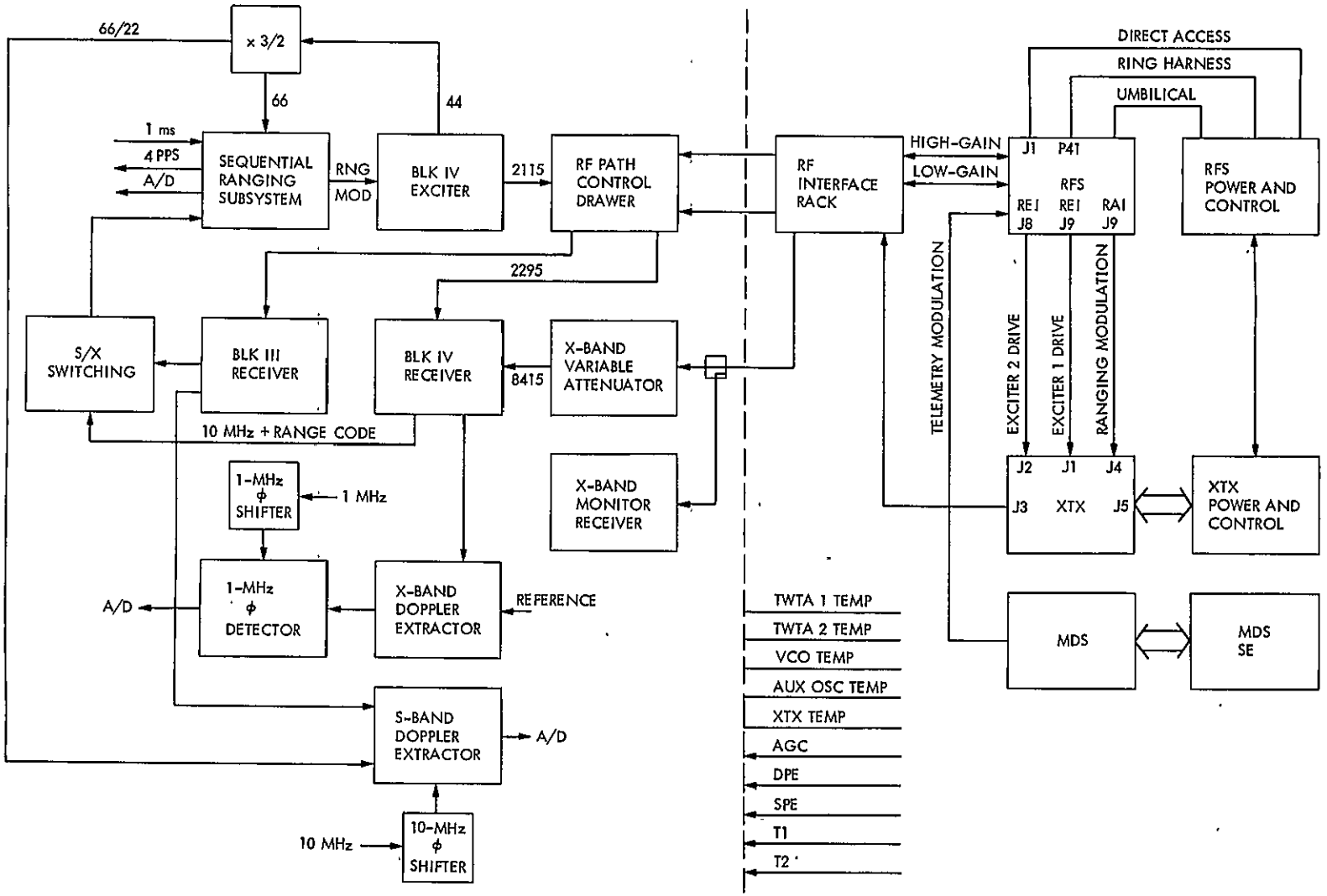

Figure 2-5. TDL S/X Test Configuration

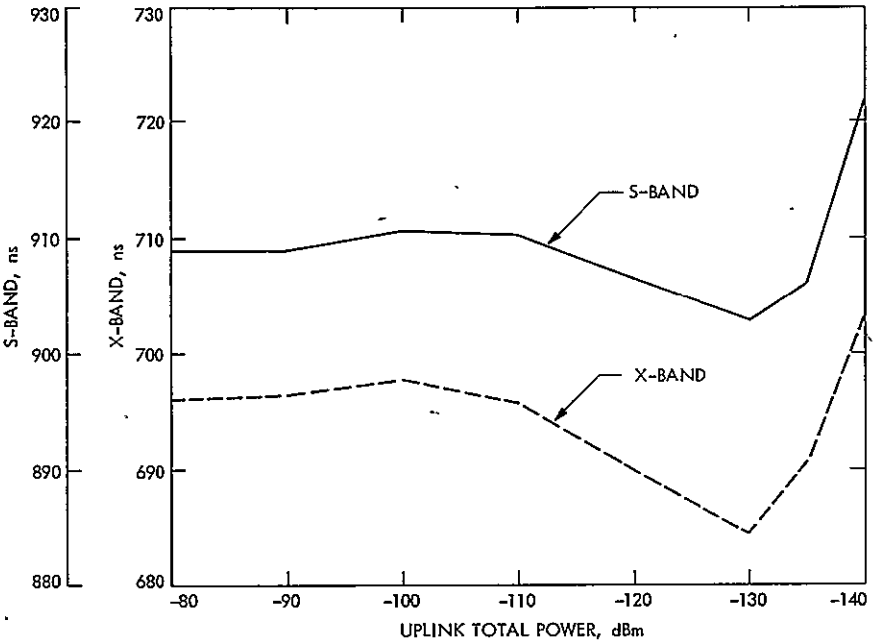

Figure 2-6. MVM'73 Flight 2 RFS/Flight SXT Ranging Group Delay vs Uplink Level

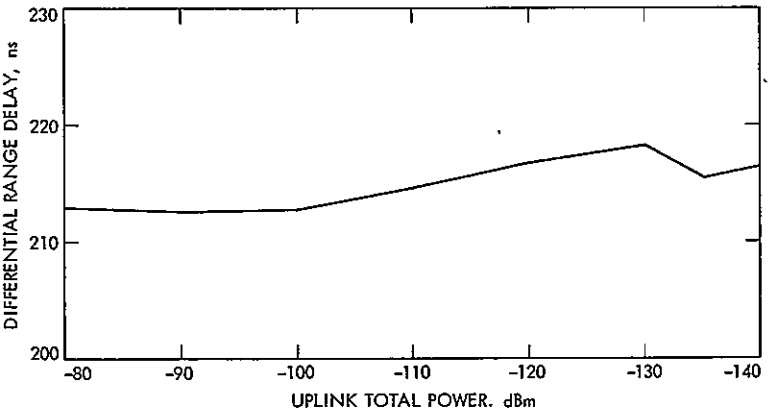

Figure 2-7. MVM'73 Flight 2 RFS/Flight XTS Differential Range Delay vs Signal Level

Group delay versus temperature is shown in Fig. 2-8. The slopes are approximately 0.22 and 0.64 ns/°C for S- and X-band, respectively.

Group delay as a function of telemetry operating mode was measured and was found to be invariant.

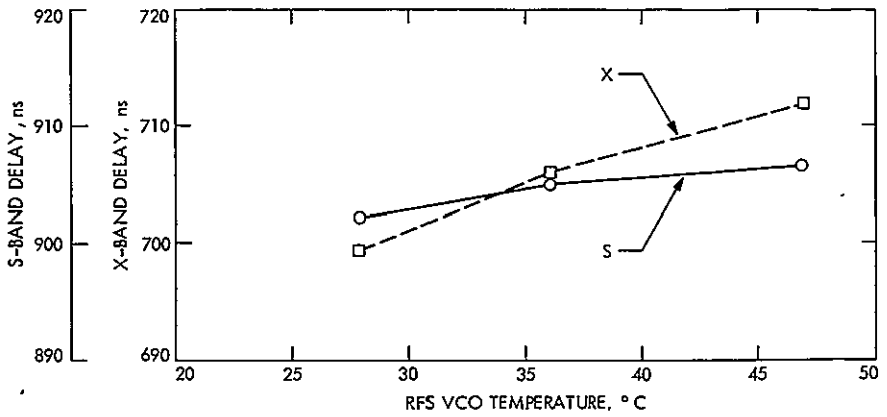

Figure 2-8. MVM'73 Flight 2 RFS/Flight XTX Ranging Group Delay vs Temperature

J. PHASE DELAY CALIBRATIONS

S/X phase delay measurements were performed for selected radio operating modes under conditions of slowly varying chamber temperature. To assure reasonably constant temperature distribution throughout both subsystems, the temperature rate was held to approximately 5°C/h. At this rate, a considerable amount of time was required to complete a temperature sweep over the normal flight approval (FA) range of 0 to 55°C. Therefore, the temperature sweep was limited to 20 to 50°C, which was the anticipated temperature range for cruise and encounter phases. The S/X ranging channel was off for all phase tests.

The procedure followed for each temperature sweep was to allow approximately 2 h of stabilization of 20°C in the selected radio mode. Data acquisition began 30 min prior to start of sweep and was continuous throughout the test.

A considerable amount of data was generated by operating on each of the parameters or in determining correlations between parameters. The most significant data is that which relates differential phase to the temperature transducers since these were the in-flight observables. A complete typical set of data, including the raw data plots, is shown in Fig. 2-9. The data shown is for the radio mode 024 (exciter 1, traveling-wave tube amplifier (TWTA) 1, high-power mode, ranging off, and transmitting via high-gain antenna port). The temperature plots show that temperature distribution is reasonably uniform throughout the radio subsystem and the XTX temperature tracks well with the RFS. Note that the actual flight transducers were being monitored.

Switching exciters or TWTAs or going from low power to high power significantly altered the rate of divergence of the two phases and even caused sign reversal. The magnitudes of the changes are relatively small and probably represent a worst case compared to the in-flight environment. The spacecraft temperature changes during any 12-h period are much smaller in magnitude and rate; hence the effect upon the electron content change measurement was expected to be very small indeed.

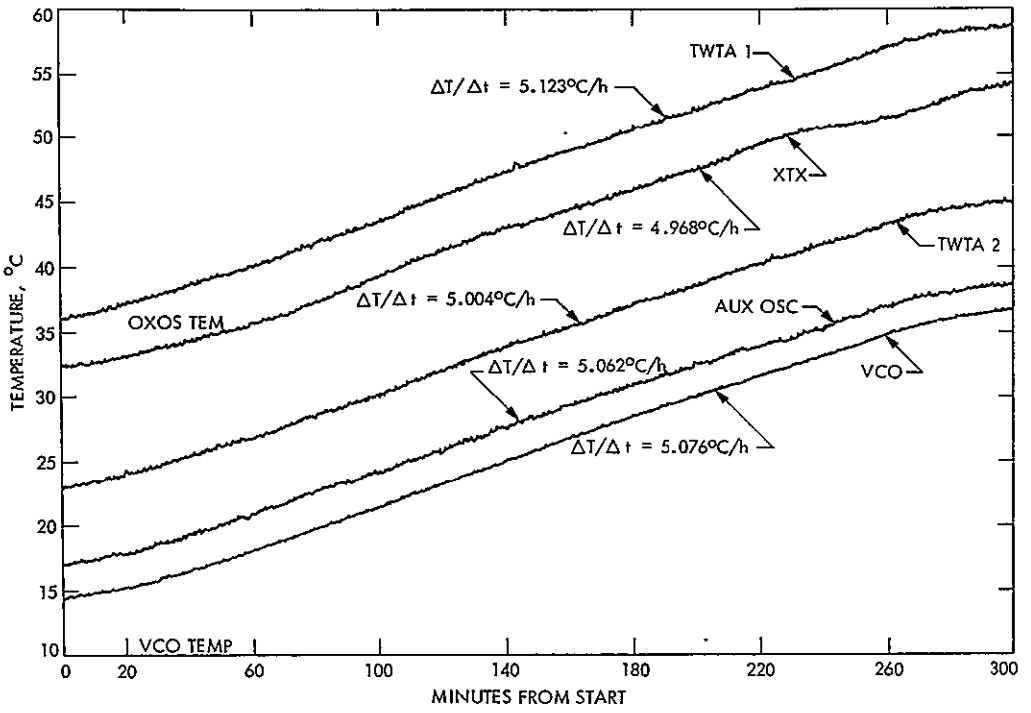

Figure 2-9. XTX Temperature Transducer vs Chamber Temperature

All RFS and XTX parameters measured in the TDL were found to be within specification. The performance of the subsystems operating in conjunction with engineering models of the ground tracking equipment indicated that the objectives of the MVM'73 radio experiment would be met.

K. THERMAL VACUUM TESTING

The most realistic prelaunch test of the S/X system was performed in the thermal vacuum environmental test chamber between July 18 and 23, 1973 (Ref. 2-11). The test configuration was the same as that shown in Fig. 2-4 with the spacecraft in the thermal vacuum chamber. The test consisted of three major events of concern to the S/X system: (1) thermal simulation of solar radiation increased from that at 1 AU (1 sun) to twice that radiation level (2 sun); (2) increase from 2 sun to 4.8 sun (the level expected at Mercury encounter), and (3) Mercury solar occultation. Differential phase measurements were made during these periods with the S/X SE. The sudden changes in sun intensity are not characteristic of our solar system; hence the thermal transient induced represents an extreme worst case. The effect upon the differential phase measurements after each of the intensity changes is shown in Table 2-2. As may be seen, the phase changes are extremely small. The major change of 11.9 deg was probably due to switching TWTAs rather than the illumination intensity shift.

Table 2-2. Differential Phase Change vs Variation in Sun Simulated Intensity

Event	Measurement time after event	Total change in differential phase
1 sun to 2 sun and switch from TWTA 1 to TWTA 2	4 h 42 min	11.9
2 sun to 4.8 sun	2 h 33 min	1.0
Sun occultation	2 h	0.5

One of the major radio science objectives was detection of Mercury's atmosphere. This was to be done by measurement of the differential phase change as the radio waves propagate through the atmosphere prior to and after earth occultation. A major concern was what the effect of the solar occultation (which occurs just prior to earth occultation) would be on the differential phase measurement. As seen from Table 2-2, the effect was negligible. This result is attributed to the combination of the good phase tracking of the S and X exciter chains and the large thermal inertia of the spacecraft.

Since differential phase measurements were performed only during a station view period (8 to 12 h) and large thermal transients (such as induced during thermal vacuum testing) were not to be expected, it was concluded that the spacecraft equipment stability was adequate to support the CMRS goals.

L. THE SPACECRAFT ANTENNA SYSTEM

The spacecraft antenna system (SXA) consisted of a high-gain antenna, a low-gain antenna, and a high-gain antenna probe assembly (Ref. 2-12). The high-gain antenna was a focal point fed 1.37-m paraboloidal reflector. The feed was a circularly polarized coaxial design. The central cavity consisted of an open-ended X-band circular waveguide. Circular polarization was achieved by loading the circular waveguide with capacitive pins to produce a quarterwave plate. The S-band portion of the feed was built coaxially, with the X-band feed in the center. The S-band cavity was fed by two probes at 90 deg from each other. The power input from the transmitter was divided in a stripline hybrid, which was built into the feed structure. The hybrid circuit gave the two probes a 90-deg phase quadrature. Figure 2-10 is a photograph of the SXA high-gain antenna feed. The high-gain antenna was the only antenna on the spacecraft capable of transmitting X-band.

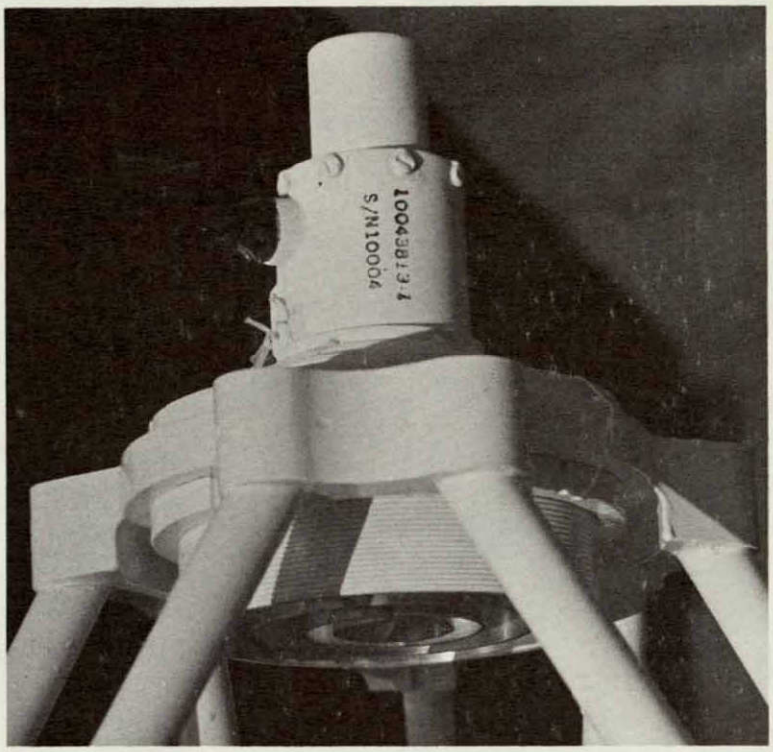

Figure 2-10. SXA High-Gain Antenna Feed

The low-gain antenna was a biconical horn fed by a slotted cylinder formed from the outer conductor of the rigid coaxial transmission line which also served as a support boom. The low-gain antenna was used for all uplink reception. It was never used for transmission in the S/X mode. The high-gain antenna probe was used for prelaunch RF testing.

M. DSS 14 S/X CONFIGURATION

The Deep Space Network 64-m antenna tracking station at Goldstone, California, was used for all the X-band investigations (Fig. 2-11). The microwave feed system was modified to permit simultaneous transmission of S-band and reception at both S- and X-band. The major design constraint for the microwave optics system was that there be no degradation below the S-band-only performance prior to the modification. This requirement was met (Refs. 2-13, 2-14, 2-15).

The system employed combined a pre-existing S-band feed system with a new X-band feed. The 64-m antenna feeds were mounted in a tricone structure (Fig. 2-12a, b). In the original tricone geometry,

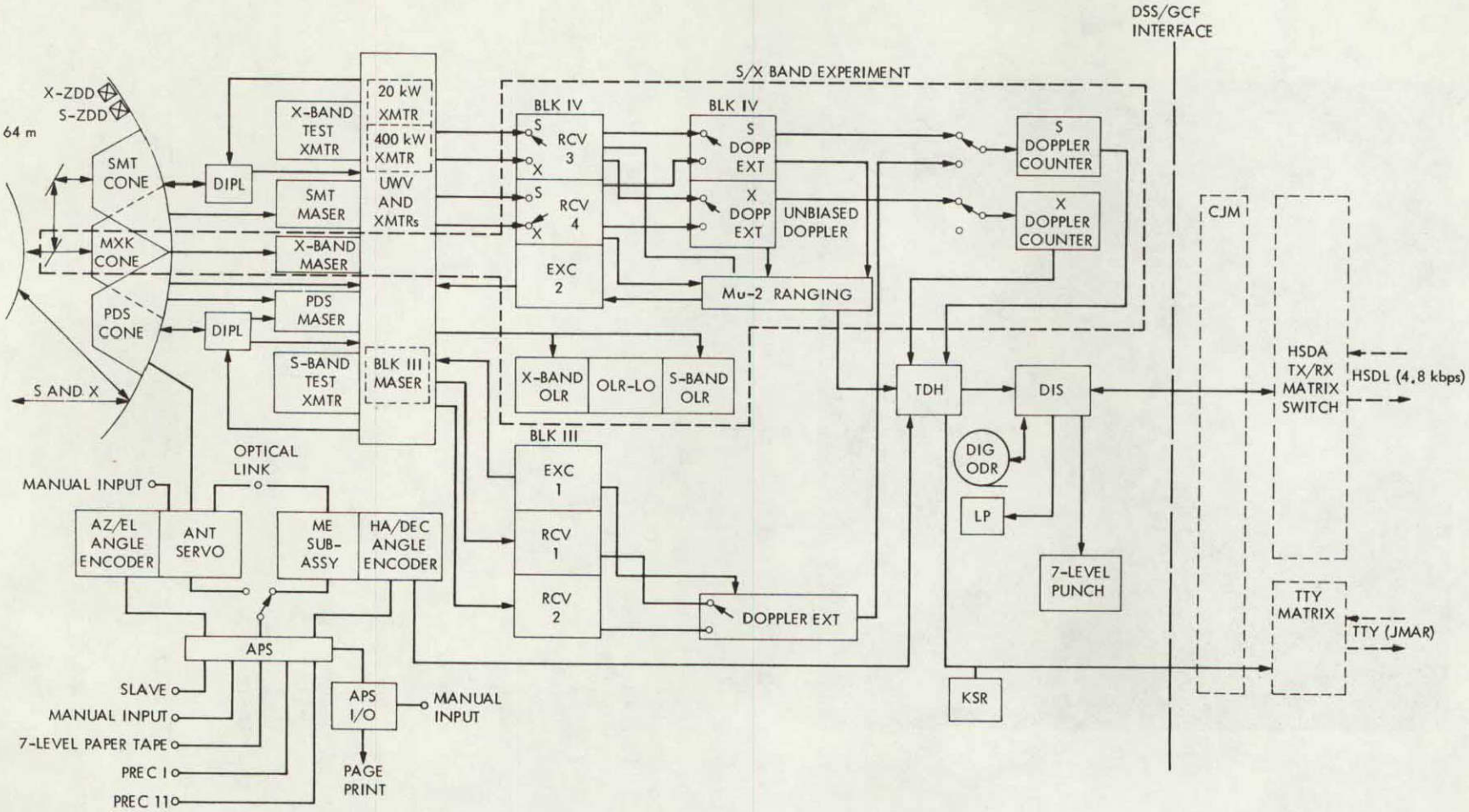

Figure 2-11. DSN Mission Configuration MVM-73 Tracking System, DSS 14

Figure 2-12a. NASA/JPL 64-m Ground Antenna with Tricone Feeds

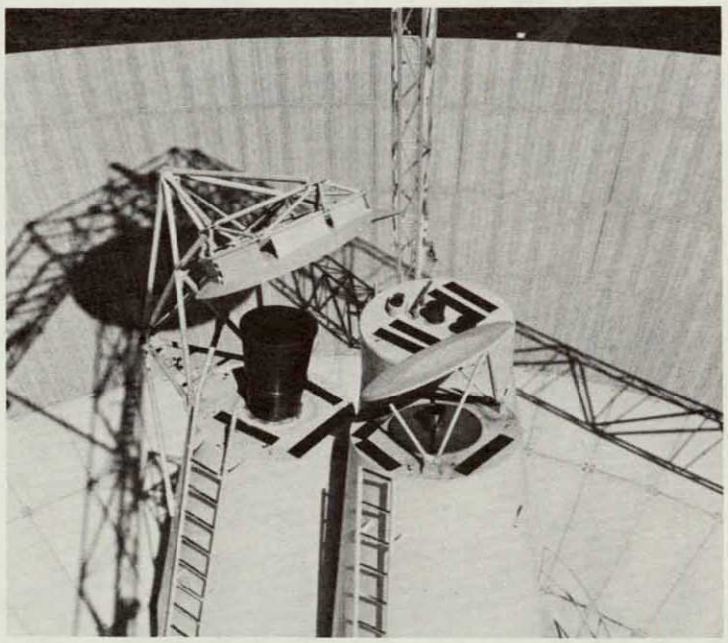

Figure 2-12b. Detail of Tricone Feeds for S-, X-, and K-Bands

one of the three feeds would be at the convex focus of the hyperboloid. The hyperboloid could be rotated so that any one of the three feeds could be in focus. The reflex feed system permitted a virtual phase center of the S-band horn to be translated so that it would be coincident with the X-band feed phase center. This was done by using an ellipsoidal reflector over the S-band feed and a dichroic reflector over the X-band feed (Figs. 2-13, 2-14). The planar dichroic reflector was transparent to X-band and reflective at S-band. Since S-band was the prime communication frequency, all performance tradeoffs at the two bands were made to optimize S-band performance.

The output of the S-band feed went to a newly designed maser using a shortened and cooled input transmission line, which resulted in a maser temperature of 2.1 K. Superconducting magnets were used to provide the maximum phase stability by eliminating interactions with the earth's magnetic field as a function of antenna orientation (Ref. 2-16). The X-band signal went to a traveling-wave maser with a noise temperature of 6.5 K. Push-pull pumping resulted in complete saturation and improved stability over previous X-band masers (Ref. 2-17). This maser also used a superconducting magnet.

From the masers, the signals went to the new Block IV receivers. These receivers were designed for maximum stability of both phase and group delays. The Block IV receiver is a quadruple conversion, superheterodyne, phase-locked receiver capable of either S- or X-band operation. Figure 2-15 shows a basic block diagram of the receiver (Ref. 2-18).

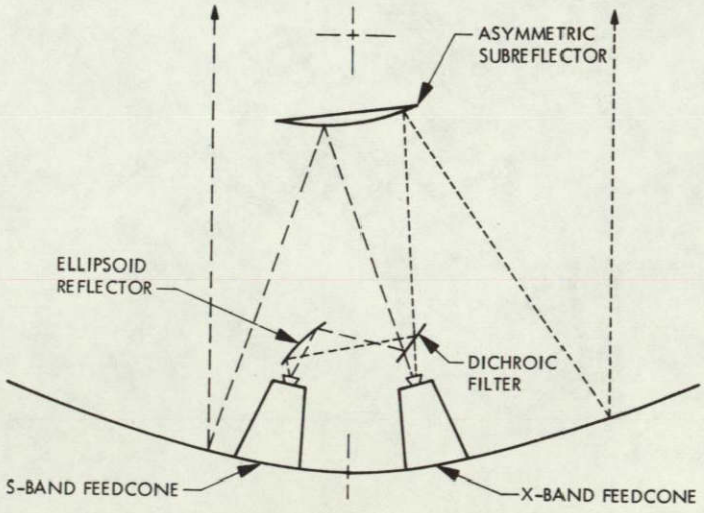

Figure 2-13. Conceptual Reflex-Dichroic Feed System

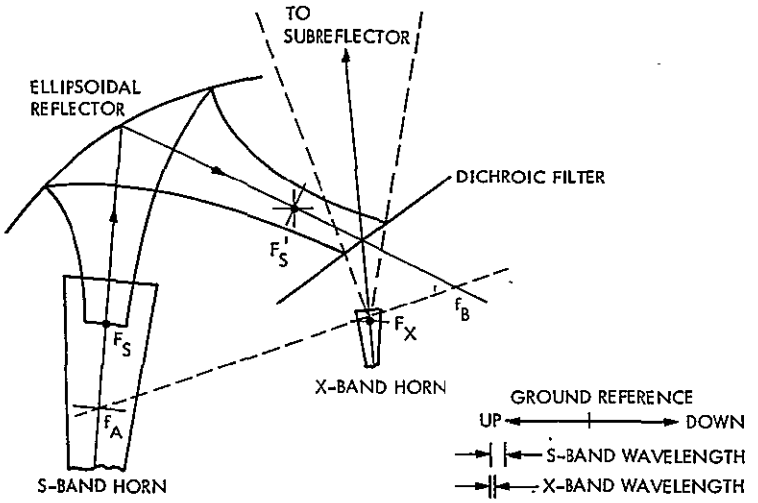

Figure 2-14. Detail of Reflex-Dichroic RF Optics

The incoming signal is converted to a first intermediate frequency (IF) of 325 MHz and then mixed down to a second IF of 55 MHz, where a non-gain-controlled output is made available for noise temperature measurements or radio science experiments. The signal is then coherently automatic gain controlled (AGC'd) to provide three constant signal level outputs at 55 MHz. The 55-MHz IF is mixed with a 45-MHz reference to generate a third IF frequency of 10 MHz.

One outstanding feature of the exciter and Doppler extractor is the inclusion of an exciter reference multiplier chain. This chain is a low-level, ultrastable multiplier that provides a stable reference to which the exciter or the klystron amplifier output may be phase-locked to provide maximum long-term phase stability of the transmitted signal. In addition, the exciter reference multiplier, when mixed with the output of the appropriate frequency shifter, provides the translated exciter frequency as a reference to the Doppler extractor. Mixing this signal with the receiver local oscillator (LO) yields a representation of the true S- or X-band Doppler for further processing. This technique of extracting the Doppler at S- and X-band allows the carrier tracking loop to track out any drift in the receiver LO multiplier chain so that these drifts do not appear in the Doppler output. This feature is very important in maintaining long-term Doppler stability. With the exciter transmitting at S-band, Doppler can be extracted from one receiver operating at S-band and another operating at X-band in the S/X mode.

A new dual-channel ranging system called Mu-2 was designed, constructed, and installed to permit accurate and flexible absolute and differential range measurements (Ref. 2-19).

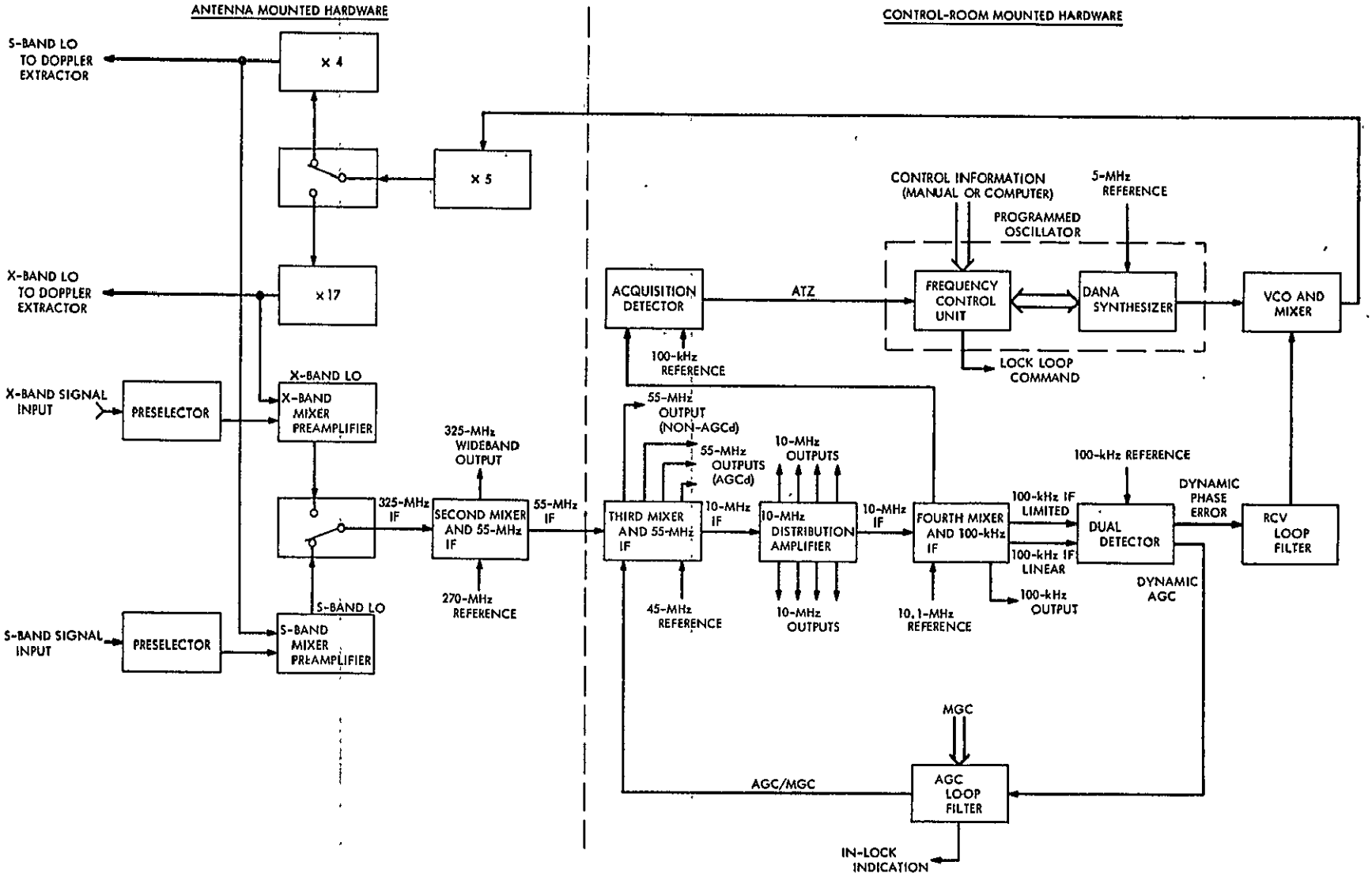

Figure 2-15. Basic Receiver Block Diagram

The relationship of the Mu-2 to other ground-based subsystems and to the spacecraft is shown in Fig. 2-16. The ranging process starts with the generation of the range code in the transmitter coder. Derived from a 66- or 132-MHz frequency reference by successive division by powers of two, the appropriate code is selected by the ranging computer. This code is phase modulated onto the uplink carrier and transmitted to the spacecraft. A transponder aboard the spacecraft, which is phase-locked to the uplink carrier, multiplies the carrier frequency by 240/221 and 880/221 to develop, respectively, S- and X-band coherent downlink carriers. Concurrently, the received range code is coherently detected, filtered in a 1-MHz passband channel, hard-limited, and used to remodulate the two downlink carriers. Note that the two-way doppler will be affected by the carrier frequency multiplication, whereas the range code will not. The downlink signals are received by two Block IV receivers, phase-locked respectively to the S- and X-band carriers. These receivers provide 10-MHz IF signals modulated with the range code to the Mu-2. Utilizing these codes, the Mu-2 independently measures the S- and X-band range. The Mu-2 has two separate and identical receiving channels, one for S-band and one for X-band.

The maximum-frequency ranging code used in the MVM mission was 500 kHz. Lower-frequency components were used as required to remove range ambiguities.

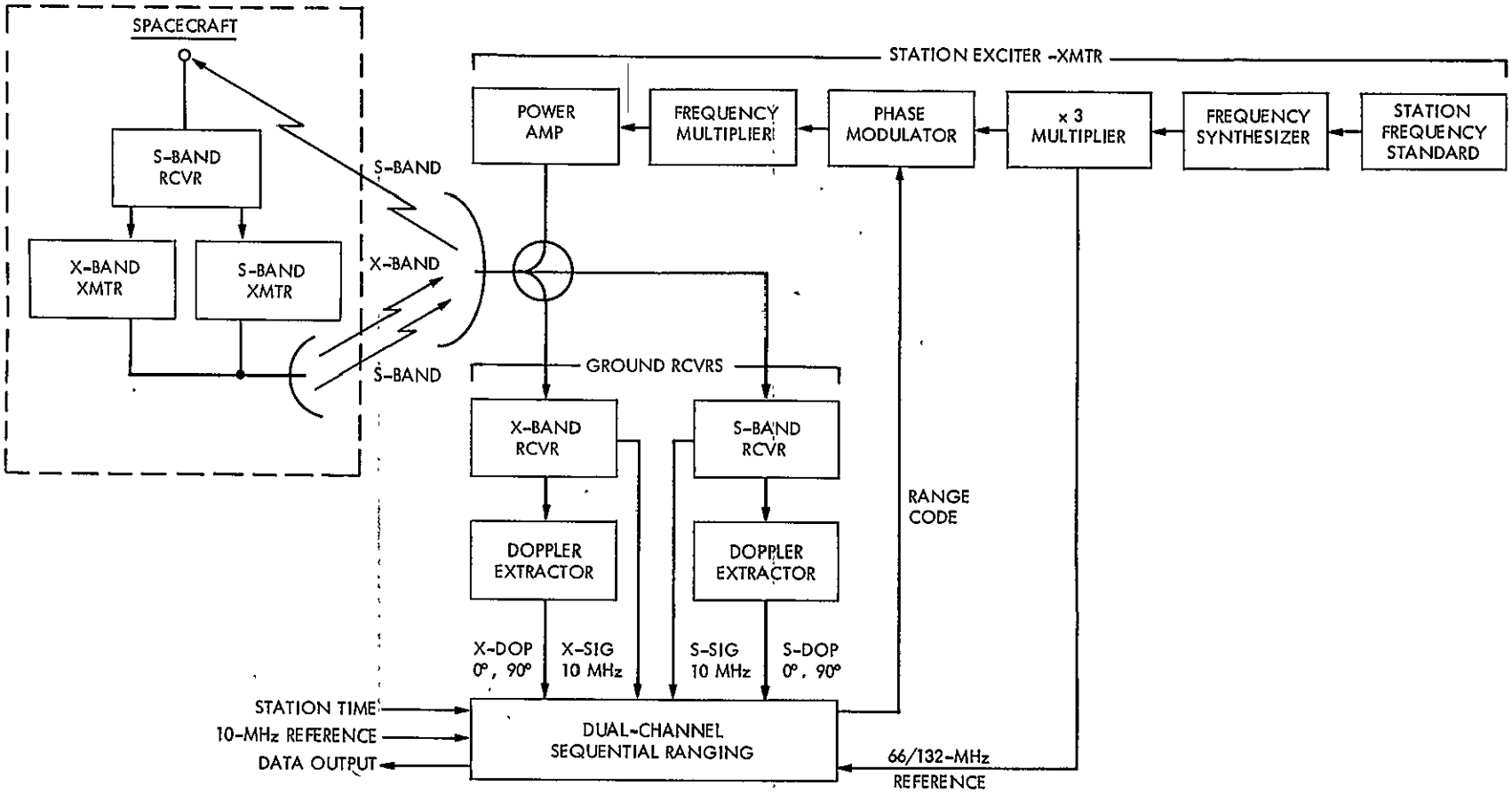

Figure 2-16. Station-Spacecraft Ranging Configuration

SECTION III

MISSION OPERATIONS

A. S/X-BAND MISSION OPERATIONS

The S/X-band system functioned will within specifications for the Venus and Mercury encounters. During the cruise phase of the mission, however, antenna pointing and ground receiver problems were experienced.

The SXA half-power beamwidth was 1.9 deg for X-band and 6.3 deg for S-band. Since the primary communication frequency was S-band, the major emphasis in attitude control requirements was for satisfactory pointing of the S-band high-gain antenna. In flight operations, the high-gain antenna pointing proved to be a major problem at X-band. One cause was the relatively coarse increments in the antenna pointing updates. This in turn was due to memory storage limitations on the spacecraft and the requirement for storing all commands for an "automatic mission."

The ground software for generating update pointing commands was very time-consuming and therefore resulted in severe limitations on the number of commands generated during the mission. Figure 3-1 shows the received X-band signal level as measured by the automatic gain control voltage. The 3-month curves are the predicted value and the upper and lower tolerance limit (Ref. 3-1).

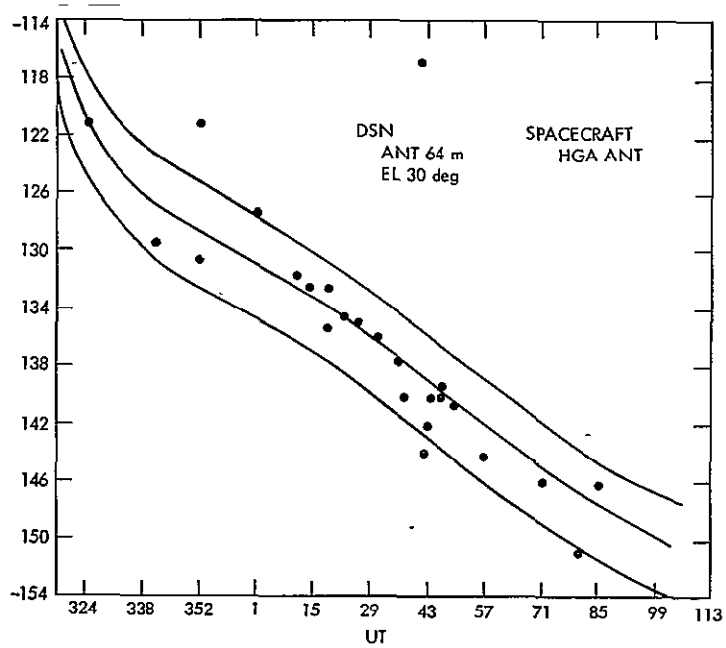

Figure 3-1. X-Band Received Signal Level

The S/X receiving system at DSS 14 was a research system which was not originally scheduled for mission support. The greater accuracies required for the radio science experiment made the use of the untested Block IV receiver necessary.

Installation of the R&D S/X-band equipment, except for the Command Modulator Assembly switch, was completed at DSS 14 in late October 1973. However, completion of checkout and an operable status were not achieved by January 1, 1974, as planned, due to a number of problems. First, S/X-band checkout during November-December 1973 at DSS 14 was very difficult and at times impossible because of conflicts with the load, configuration control, and freeze imposed at the station for Pioneer 10 encounter. Secondly, subsystem interface cable noise problems and faulty assembly modules further delayed achievement of valid data. Most problems exhibited themselves in the X-band rather than S-band data in the form of frequency Doppler cycle slips and offsets (Ref. 3-2).

The antenna pointing problem at the ground station was virtually eliminated by employment of a semiautomatic conical scan tracking technique using the antenna pointing system computer (Ref. 3-3).

On December 25, 1973, the spacecraft high-gain antenna experienced partial failure, resulting in a drop of observed RF power. The high-gain antenna was observed to experience a number of fail-heal-fail cycles during this period. Degradation of the downlink varied from 2 to 6 dB below the design value, and the resulting signal polarization was linear rather than the normal circular. Approximately 3 dB of the high-gain antenna loss was attributed to the cross-polarization between the circular polarization of the deep space station antennas and the nearly linear polarization of the spacecraft. In response to the Project's request, and to meet Mercury TV experiment objectives, the Deep Space Network initiated emergency action to provide, ship, and install linear polarization equipment at each of the three 64-m stations. This task was planned to be completed shortly before Mercury encounter.

Concurrently with these critical events, the Project and the DSN pushed on with some planned experiments. Using DSS 14, an X-band telemetry data experiment was conducted wherein data were modulated on the uplink ranging channel. The spacecraft turned these data around much like the ranging code on the S/X-band downlink. Therefore, DSS 14 then used the Block IV receiver to acquire the S/X-band signal containing telemetry data, thus giving a measure of the X-band frequency performance for telemetry transmission. This experiment was conducted on January 11 and again on January 15, 1974.

Shortly prior to Venus encounter, ground and flight test data showed that the spacecraft auxiliary oscillator had a frequent one-half-cycle offset when operating in the one-way mode. Instability

of this nature would have masked Venus' atmospheric effects on the RF signal, thus severely degrading radio science occultation results. It was determined that proper auxiliary oscillator performance could be obtained in the two-way mode, but to do this required use of the newly implemented 100-kW transmitter at DSS 14 to gain adequate link performance. Furthermore, the Venus near-encounter sequence had been planned to be conducted in a one-way, listen-only mode to enhance performance for high-rate video acquisition. The decision was made in favor of radio science support, and the DSN with the Project had to develop a new two-way, 100-kW sequence between February 1, 1974, and Venus encounter on February 5. Detailed planning and coordination continued until Venus encounter minus 1 day (Ref. 3-4).

On February 5, 1974, at 17:01:04 GMT (spacecraft time), the Mariner 10 spacecraft reached closest approach to the planet Venus. Closest approach activities were visible only to the Goldstone complex, thus limiting participation to DSS 14 (the prime site) and DSS 12 (the backup site), and was noteworthy from a tracking system standpoint in that it marked the first use of the Block IV S- and X-band receiver (at DSS 14) during a critical phase of a planetary encounter.

An important factor of the Venus encounter was the extremely large refractive effect of the Venusian atmosphere during the period between geometric enter and exit occultation. (At its peak, this refraction amounted to approximately 13 kHz, two-way S-band.) This refractive effect evidenced itself very strongly during the pre-encounter tracking operations planning phase in three areas:

(1) As the signal refraction increased, its attenuation increased and, as no information existed regarding the accuracy of the attenuation data, uncertainty arose as to when lock would drop and when spacecraft uplink and downlink would be reacquired.

(2) No information was available regarding the accuracy of the atmospheric Doppler predictions, impacting the selection of an acquisition sweep range.

(3) The DSN Prediction Program did not model planetary atmospheric refraction, so that the refraction predictions had to be manually factored into otherwise computerized prediction data for the various encounter strategy studies.

Figure 3-2 shows the S-band frequency as MVM'73 approached the planet and went into occultation. The frequency scale is relative to the nominal 2295-MHz signal transmitted by the spacecraft. If the spacecraft were receding from the earth at a uniform velocity, the downward trend would be a straight line. However, it was being accelerated by Venus' gravity field, and the downward trend was

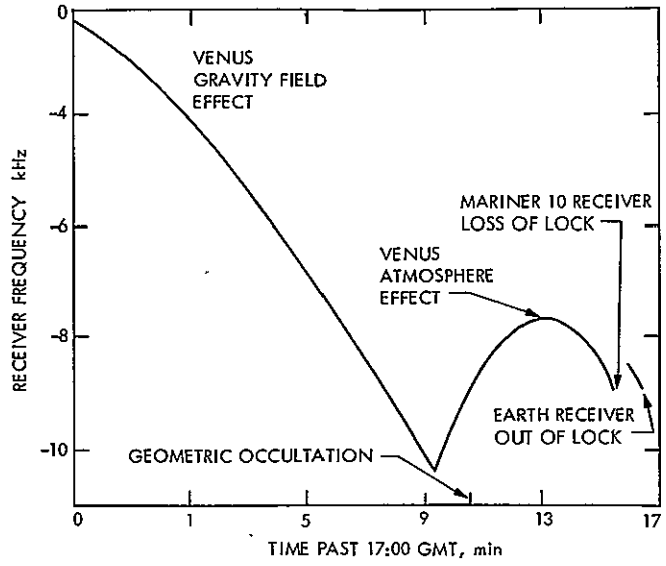

Figure 3-2. S-Band Venus Occultation Doppler Shift

increasing, causing curvature. Suddenly, as the MVM'73 radio signal hit the atmosphere, the frequency reversed direction and at the same time began to fade away. The spacecraft high-gain antenna, under preprogrammed computer control, was steered to keep the earth at the peak of the main beam. The spacecraft went behind the planet, but the signals remained locked onto by the earth receivers. About 6 min behind the planet, the spacecraft receivers lost lock of the signal transmitted from earth, and the spacecraft switched to its backup oscillator. Since its frequency is different from that on earth, the ground-based receivers lost lock--but they picked it up in less than a minute and tracked it for an additional 30 s (Ref. 3-2).

At the same time, these signals were received by some receivers that do not lock on but instead record all the frequencies of interest. These are called the "open-loop" receivers. The penalty paid for recording everything is the necessity to computer process the data later. It is a slow, but very detailed and completely adaptable technique. There is no error, for the computer can fly by the planet as many times as necessary. H. T. Howard's postprocessing of the open-loop tapes indicates that the S-band signal was detectable throughout the occultation (Ref. 3-5). Table 3-1 indicates the in- and out-of-lock times for the Venus encounter.

In summary, tracking operations during the Venus encounter phase were extremely successful, especially in light of the considerable difficulties posed by the confluence of new equipment at DSS 14 (Block IV receivers) and the large uncertainties associated with the Venusian atmospheric effects on telecommunications. The one minor

Table 3-1. Summary of DSS Receiver Events

Event	Ground received time, GMT (February 5, 1974)
Enter atmosphere[a]	17:09:10
Enter geometric occultation[a]	17:09:23
Block IV X-band out-of-lock	17:10:45
Block III prime and backup out-of-lock	17:14:58
Block IV S-band out-of-lock (two-way)	17:15:35
Block IV S-band out-of-lock (one-way)	17:16:30
Block III backup in-lock	17:25:48
Block III prime in-lock	17:26:03
Block IV S-band in-lock	17:28:58
Exit geometric occultation[a]	17:30:17
Exit atmosphere[a]	17:30:28
Two-way[a]	17:32:50
Block IV X-band in-lock	17:40:58

[a]Best estimates from actual encounter data.

problem during this phase was the late acquisition by the Block IV receivers at exit occultation, which was explained in large part by the unexpectedly lengthy lock at enter occultation and a degree of unfamiliarity with the new equipment. Furthermore, the late acquisition entailed no loss of data since

(1) The DSS 14 Block III receivers locked up extremely early in the exit occultation, successfully receiving all spacecraft data.

(2) The DSS 14 open-loop receivers successfully acquired data during both enter and exit occultation, thus satisfying radio science requirements.

The geometry at Mercury during the MVM'73 occultation as seen from earth is shown in Fig. 3-3. Conduct of the experiment was nearly identical to that described for Venus encounter.

On March 29, 1974, at 20:46:31.9 GMT (spacecraft time), the spacecraft reached closest approach to the planet Mercury. This encounter was simultaneously visible to both the Goldstone and the Australian complexes, thus allowing prime participation by two 64-m deep space stations, DSS 14 and DSS 43. Significant elements of the configuration at the stations during the encounter included the Block IV S- and X-band receivers at DSS 14 and the digital controlled oscillators and open-loop receivers at both DSS 14 and DSS 43. The following combination of circumstances contributed to improving tracking operations results:

(1) Mercury has essentially no atmosphere, thus greatly reducing the signal refraction and the corresponding uncertainties in the times of and Doppler at enter and exit occultation.

(2) The mass of Mercury is relatively small, thus inducing only a small perturbation in the near-encounter Doppler.

(3) Although the Block IV receivers and the digital controlled oscillators were relatively new, considerable operational experience with them had been obtained in the previous 4 to 6 months, and especially during the Pioneer 10 Jupiter and MVM'73 Venus encounters.

(The positive effects of the first two were anticipated.) Table 3-2 presents the times of critical Mercury encounter events.

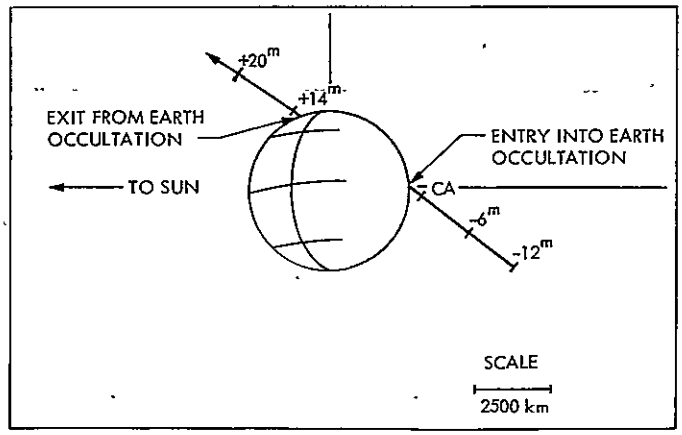

Figure 3-3. Geometry of Mercury Occultation

Table 3-2. Spacecraft and DSS Events During Mercury Occultation

Event	Ground received time, GMT (March 29, 1974)
Enter occultation	20:56:11.69
DSS 43 drop lock	20:56:12
DSS 14 S-band Block IV drop lock	20:56:12
DSS 14 X-band Block IV drop lock	20:56:12
Exit occultation one-way	21:07:33.03
Downlink one-way to two-way	21:07:43.55
DSS 43 acquire downlink	21:07:46
DSS 14 S-band Block IV acquire downlink	21:07:46
DSS 14 X-band Block IV acquire downlink	21:09:56

On March 31, 1974, at the start of an outgoing TV mosaic sequence, a spacecraft power subsystem problem occurred which resulted in large power dissipations in the spacecraft bus. The voltage transients which accompanied this event caused the transmitter to exhibit two failure modes. One was a spectrum consisting of a discrete carrier suppressed by approximately 2 dB, with odd harmonic nonsymmetrical sidebands spaced approximately 5.6 kHz from the carrier. In this mode, all telemetry indicators were normal and normal tracking and ranging could be achieved. The second mode resulted in a spread spectrum in which the carrier was suppressed by at least 20 dB and there were no measurable sidebands. In this mode, the output power telemetry monitor read low, and the ground receivers could not lock to the signal.

Bench tests at Motorola were able to reproduce these modes by failing certain components in the XTX dc-dc converter. The consensus was that the failure was caused by a large power transient.

It was found that operationally the XTX would be caused to recover from the spread spectrum mode by either momentarily turning the unit off or by going from two-way to one-way and then back to two-way transmission. This was accomplished by momentarily turning off the ground transmitter (Ref. 3-6).

B. EXTENDED MISSION

The ability of the S/X system to measure total path electron content made the extended mission extremely interesting from the Radio Science Team's point of view. At the time of solar superior conjunction on June 6, 1974, the dual-channel S-band and X-band radio signals emanating from MVM's high-gain antenna passed within 1.67 deg of the sun's surface as viewed from earth. Effects of the solar corona's electron cloud on these signals were recorded at DSS 14 using open-loop receivers and the R&D Block IV closed-loop receivers. Primary effects of the solar corona on the radio signals were scintillation and differential S/X-band group delay. MVM'73 was the first space mission in which an X-band signal was used to probe the sun's environment. In addition, dual-channel S/X-band ranging data were gathered. Data quality remained good despite low signal strength and high noise conditions. The influence of the sun's coronasphere upon the range values became increasingly significant as the date of superior conjunction approached. Figure 3-4 is a plot of differential delay for the period, where it can be seen that differential delay exceeded 3 μs. The right-hand axis presents delay in terms of total electron content, and the measured content is shown to be quite variable compared to that predicted by a smooth, quiet $1/r^2$ model. Much greater delays are expected for future missions, where the sun-earth-probe angle will be smaller. The measurement will be a vital correction for relativity experimenters and of great interest to solar physicists.

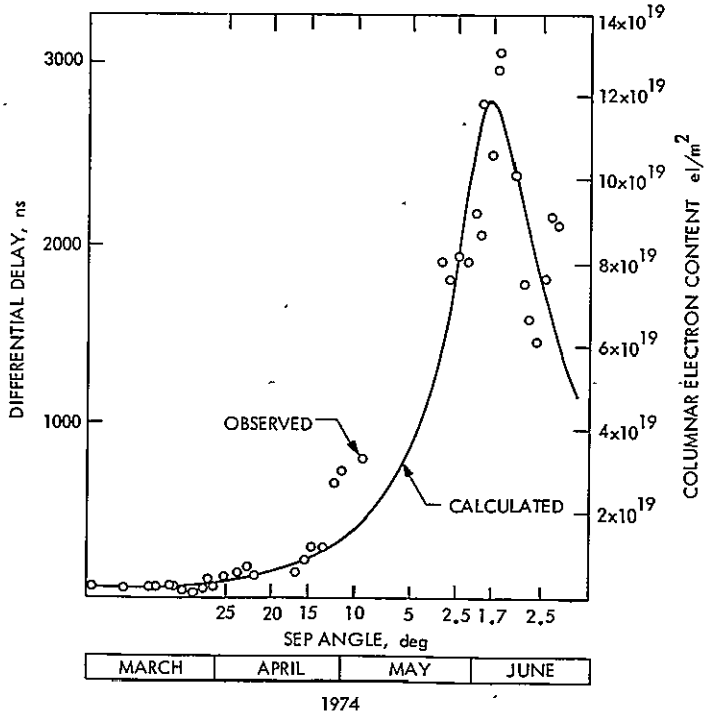

Figure 3-4. Differential Range Delay Near Superior Conjunction

MVM'73 solar superior conjunction activities occurred during the period May 24 through June 21, 1974. Recovery of dual-frequency S/X-band Doppler data, range, and open-loop receiver data types was required. In addition, it was desired that calibration tracks be provided beyond the stated intervals. Since MVM'73 provided the first opportunity for spacecraft dual-frequency analysis of solar corona and gravity effects, the DSN gave considerable emphasis to arranging proper support at DSS 14. Originally, DSS 14's Block IV S/X-band receiver was scheduled for removal and rework in preparation for Viking test support in mid-June 1974, following superior conjunction on June 6, 1974. The expanded observation period required negotiation of the removal date and was subsequently set for July 1, 1974. Support by the special Block IV receiver trouble-shooting team was planned to continue in effect until July 1, 1974. Telecommunications performance during this period was influenced by the sun-earth-probe angle, the level of solar activity, and the communications modes used.

Typically, during solar conjunction, the bit error rate increased as the sun-earth-probe angle decreased, with no total loss of data during the entire period. Also, usable two-way S-band Doppler and S-band ranging were received, although the Doppler noise level greatly increased. X-band ranging and Doppler were of limited use due to the multiplication factor in the noise on the X-band downlink.

SECTION IV

INVESTIGATION, DESCRIPTION, AND RESULTS

A. TECHNOLOGY EXPERIMENTS WITH THE X-BAND MVM SYSTEM

1. The X-Band Telemetry Experiment

The X-band telemetry experiment using the MVM'73 spacecraft and DSS 14 ground facility had the following major purpose and objectives:

(1) To demonstrate, using an in-flight spacecraft and an operational DSS, that X-band high-data-rate, convolutionally coded (plus Golay algebraic codes) telemetry data can be reliably transmitted, received, and processed in accord with performance predictions.

(2) To uncover and identify potential design or operational problems that may exist relative to the use of X-band telemetry on future spacecraft missions so that early corrective measures can be taken.

(3) To quantitatively measure the performance of the X-band telemetry link to assess the effects of weather, system temperature as a function of elevation, phase noise, coded burst-error statistics, etc., and to gain a better knowledge of performance parameters and their tolerances.

(4) To complement the MVM'73 radio science experiment by providing an assessment of short-term effects.

Two types of experiments were planned: (1) a very-high-data-rate (100 kbps) qualitative demonstration and (2) a series of quantitative experiments at a medium data rate (10 kbps). The qualitative experiment involved simulating, to the greatest extent possible, the conditions proposed for the Voyager 1977 high-rate telemetry channel.

In order to achieve the goals set for the qualitative experiment, it was necessary to conduct the experiment within the first 6 weeks of the flight of the spacecraft, or before December 15, 1973. Unfortunately, the problems involved in bringing the Block IV X-band receiver system to an operational status took priority in the time schedule, such that the qualitative experiment had to be cancelled.

The intent of the series of quantitative experiments was to gather data from both the X-band and S-band receiving systems taken over a number of days (5 to 10) for which differing conditions, especially weather, existed.

The quantitative experiment also fell victim to the delays in making ready the Block IV equipment, and more importantly, the S-band feed failure that occurred in late December 1973. As a result, only two experiment dates could be obtained: January 11 and 15. On January 11, a failure of a coupler associated with the zero-delay test transmitter configuration caused ground-generated signals to be superimposed on the received signals, thus rendering the data invalid. On January 15, a successful experiment was conducted, with 70 continuous minutes of data taken.

Figure 4-1 shows the coded and uncoded results plotted with respect to the ideal performance curves. In plotting the experimental data, the signal-to-noise ratio estimator values were used to locate the points. As a result, the uncoded symbol results appear slightly to the left of the uncoded ideal curve.

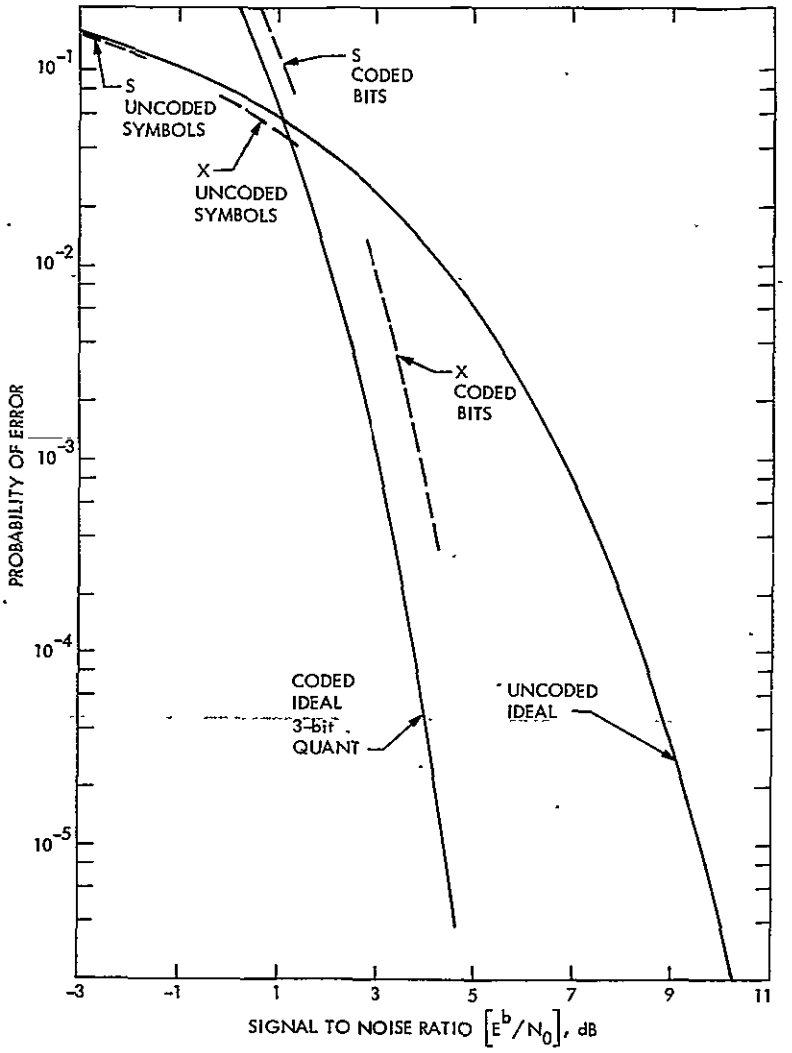

Figure 4-1. X-Band Telemetry Experiment--Probability of Error Results

As can be seen, the S-band results are about 0.4 dB to the right of the ideal coded curve, and the X-band signals are off about 1 dB in performance. The 1 dB may be accounted for by (1) the apparent non-gaussian form of the X-band channel (reason unknown) and (2) perhaps some error in scaling the signal-plus-noise into the quantizer. (The decoder performance is somewhat sensitive to this scaling.) The conclusion reached is that the nominal performance is quite good, and that given a larger set of experimental data, and time to become more familiar with all the idiosyncrasies of the Block IV X-band system, the X-band performance offset can be made comparable to that of S-band.

2. Navigation Enhancement Experiments

Two objectives of the navigation experiment were to validate the use of S/X Doppler change of electron content by comparison with Faraday rotation measurements and to show enhancement of navigational accuracy by using the differential S/X Doppler for orbit determination. Both of these objectives were met (Ref. 4-1).

S/X dual Doppler exploits the inverse-frequency-squared dependence of the phase velocity change of a radio signal traversing a tenuous plasma. The Doppler shifts present in the received S- and X-band tones measure two occurrences: the radial motion of the spacecraft as seen from DSS 14, and the net change in the total number of electrons encountered along the ray path. That portion of the Doppler shift resulting from radial motion of the probe is removed by differencing the Doppler shifts, and the balance is due to charged-particle effects. In equation form, the procedure to compute the balance is

$$\text{Balance} = \frac{K\left(S - \frac{3}{11}X\right)}{f_{q_s}}$$

In other words, the X-band frequency is multiplied down to an equivalent S-band frequency and differenced from the S-band received frequency. This difference in the net frequency change at S-band is then due entirely to electron content variations. The ratio of the S-band frequency can be easily converted to electron content variations or apparent range change to the spacecraft.

To date, only two charged-particle calibrators can achieve submeter level precision: S/X dual Doppler and Faraday polarization data. Other calibrators, differenced range versus integrated doppler (DRVID) and dual S/X range, provide charged-particle assessments to the precision of the DSN range data, which is typically in meters.

It should be noted that the Faraday rotation data are obtained from measurements to geostationary satellites. At the Goldstone DSN complex (site of DSS 12 and DSS 14), three Faraday polarimeters continuously monitor the amount of rotation experienced by the plane-polarized transmissions of the Applied Technology Satellites ATS-1 and ATS-5. These observations provide a measure of earth's ionospheric electron content and its time-rate of change. The Faraday polarization data must be mapped from the DSS-satellite line-of-sight to a planetary spacecraft. This mapping technique is based on a mathematical model (Ref. 4-2), which is frequently inadequate at low topocentric elevation angles. Typically, the uncertainty of mapped Faraday for lines-of-sight taken above 30 deg elevation is $\sim$0.1 m (1 σ). For elevation angles below 30 deg, the uncertainty is 0.3 m (1 σ).

The siutation can be stated thus: If the S/X dual Doppler data and the "mapped" Faraday polarization data show the same electron content history, within the precision of the mapped Faraday data, no plasma activity of significance is assumed to exist, and the S/X dual Doppler data are valid; if the S/X Doppler data cannot be favorably compared to the Faraday data, it is possible that the S/X dual doppler is "seeing" solar plasma activity. In short, the S/X dual doppler can be verified only if it compares to the mapped Faraday data on some occasions.

The Faraday polarization data used in these comparisons were sampled every 10 min. The S/X dual Doppler, as processed, provides only half the high-frequency resolution inherent in the data.

Comparisons of the available S/X dual Doppler and mapped Faraday data through Mercury flyby (March 29, 1974) are shown in Fig. 4-2. As can be seen, for some passes (ten in number), the dual Doppler and Faraday agree over the entire tracking pass; i.e., the two calibrations do not differ by more than 0.1 m in cumulative range error change. Some passes (twelve in number) show similar agreement for the two calibrations when the elevation angle associated with the S/X dual Doppler observation is greater than 30 deg. There are still other passes (seven in number) for which the differences between the two calibrations are in excess of 1 m. The passes shown having this character are believed to be exhibiting real space plasma effects. The following evidence supports this conjecture:

(1) S/X dual Doppler data indicated high plasma activity.

(2) The charged-particle detector aboard the spacecraft recorded high ion levels and fluctuations.

(3) S-band radio metric Doppler showed structure not related to the normal phenomena encountered.

(4) Earth's ionosphere, as measured by the Faraday polarization data, was excited. This excitement stems from the solar plasma interaction with the ionosphere. The ionosphere showed activity 2.5 times higher than the normal at times.

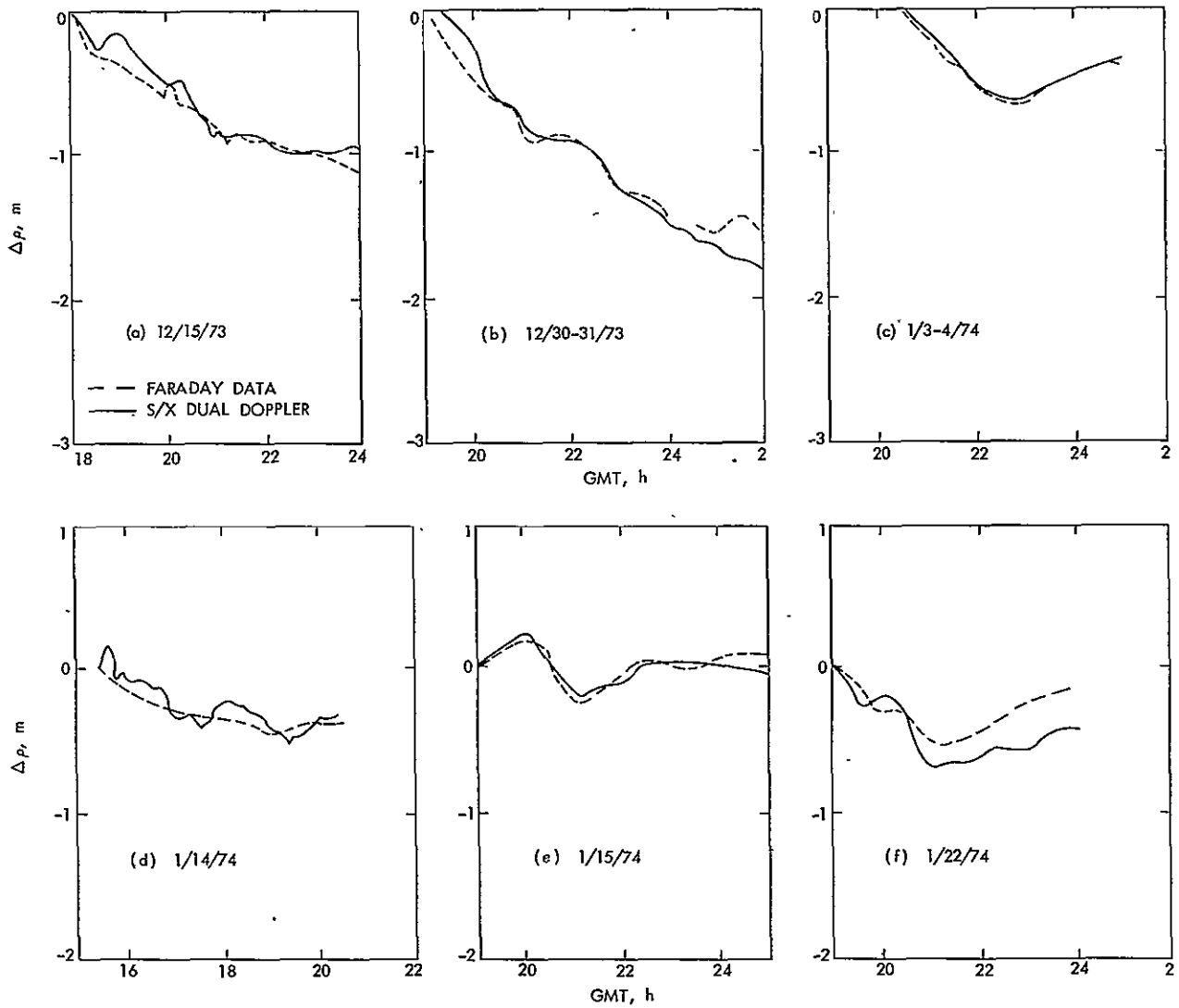

Figure 4-2. S/X Dual Doppler and Faraday Polarization Data Comparisons

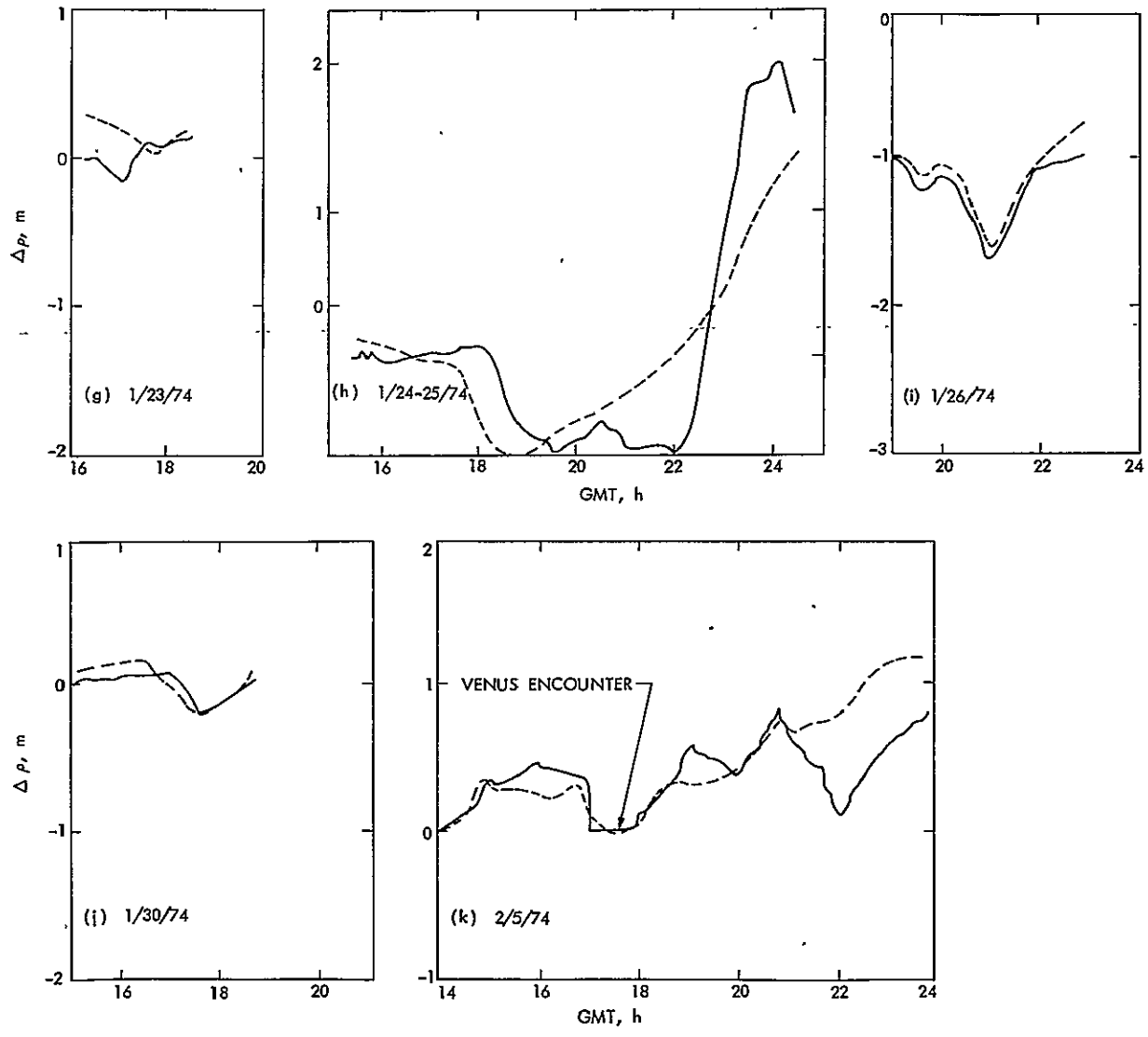

Figure 4-2. S/X Dual Doppler and Faraday Polarization Data Comparisons (Continuation 1)

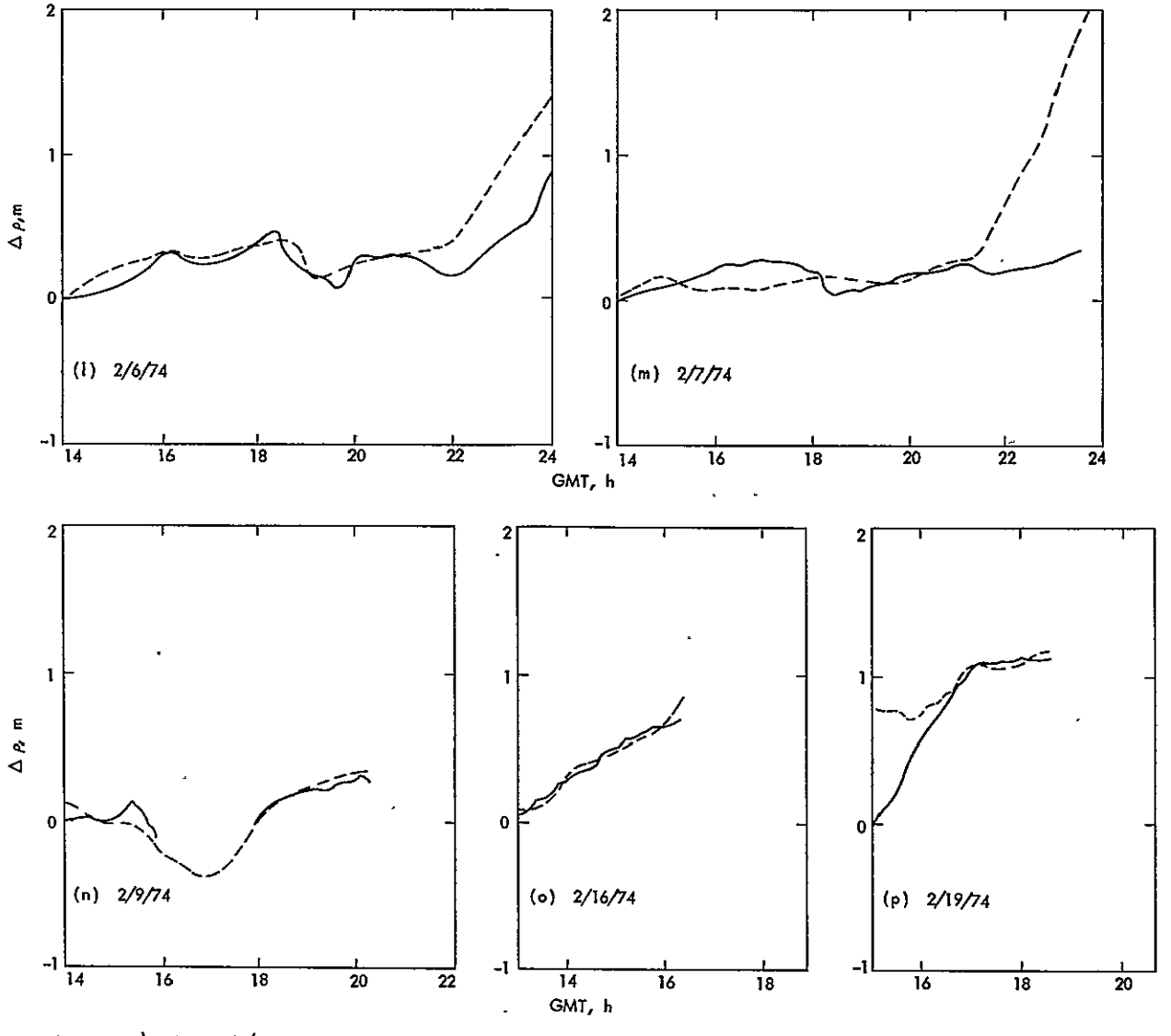

Figure 4-2. S/X Dual Doppler and Faraday Polarization Data Comparisons (Continuation 2)

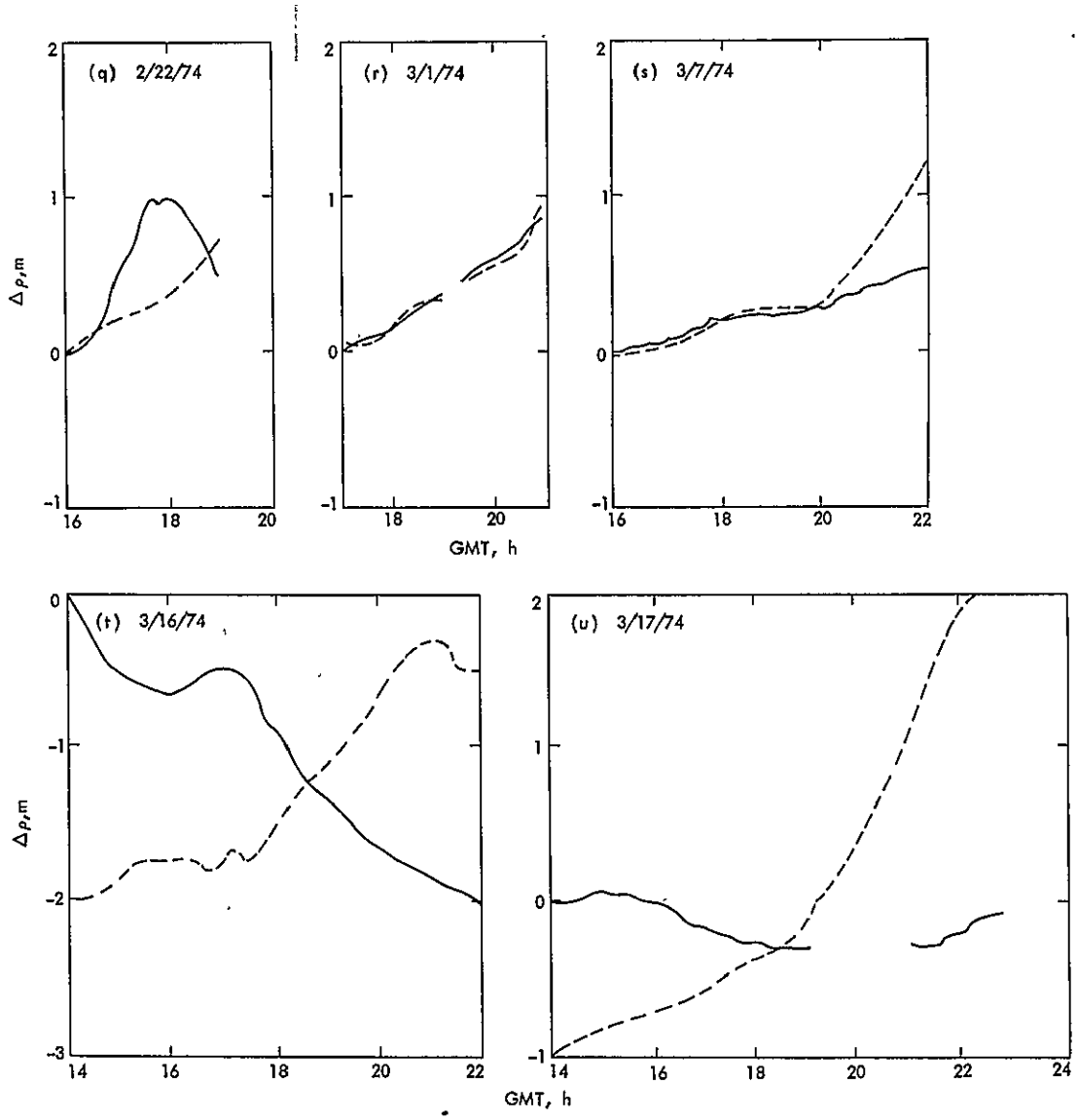

Figure 4-2. S/X Dual Doppler and Faraday Polarization Data Comparisons (Continuation 3)

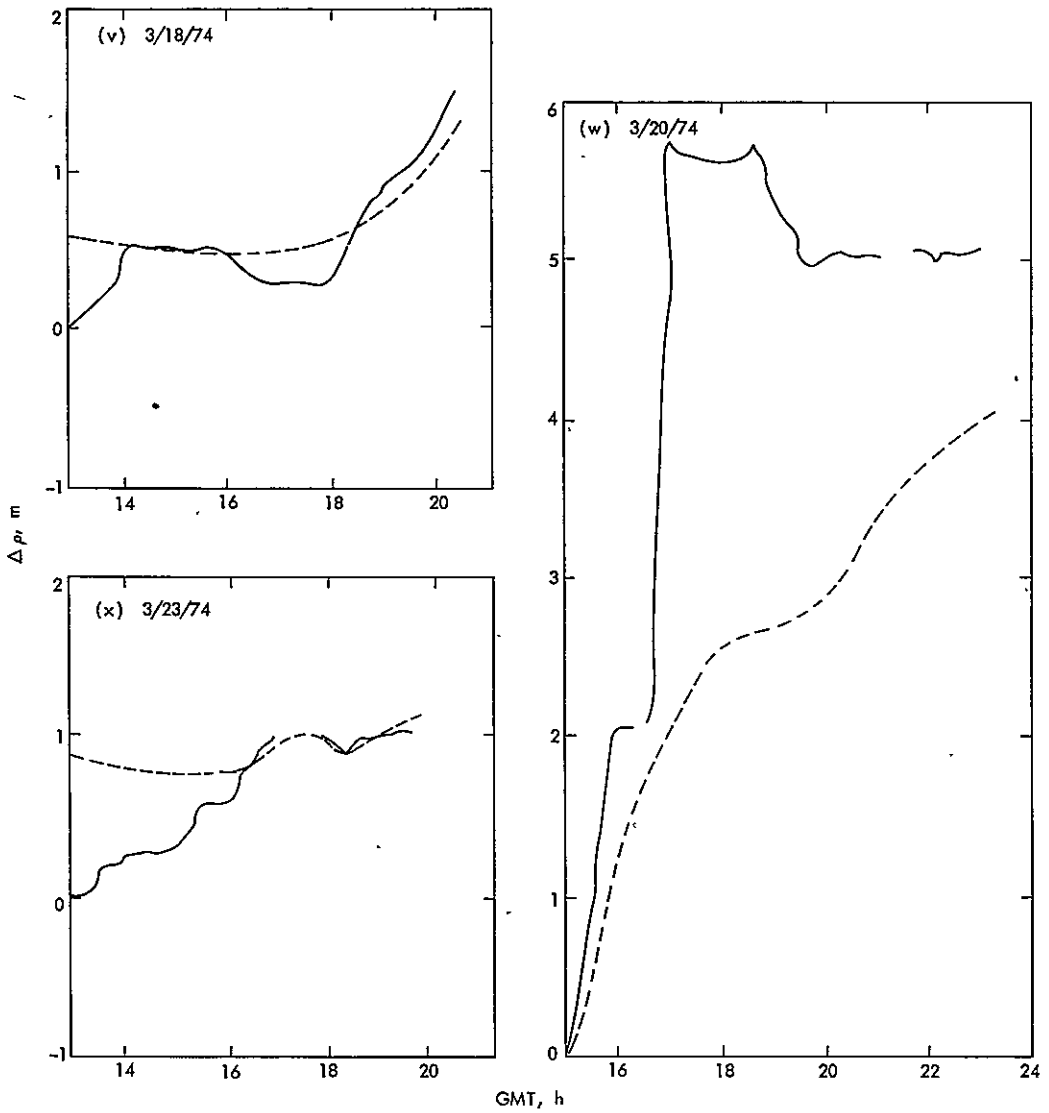

Figure 4-2. S/X Dual Doppler and Faraday Polarization Data Comparisons (Continuation 4)

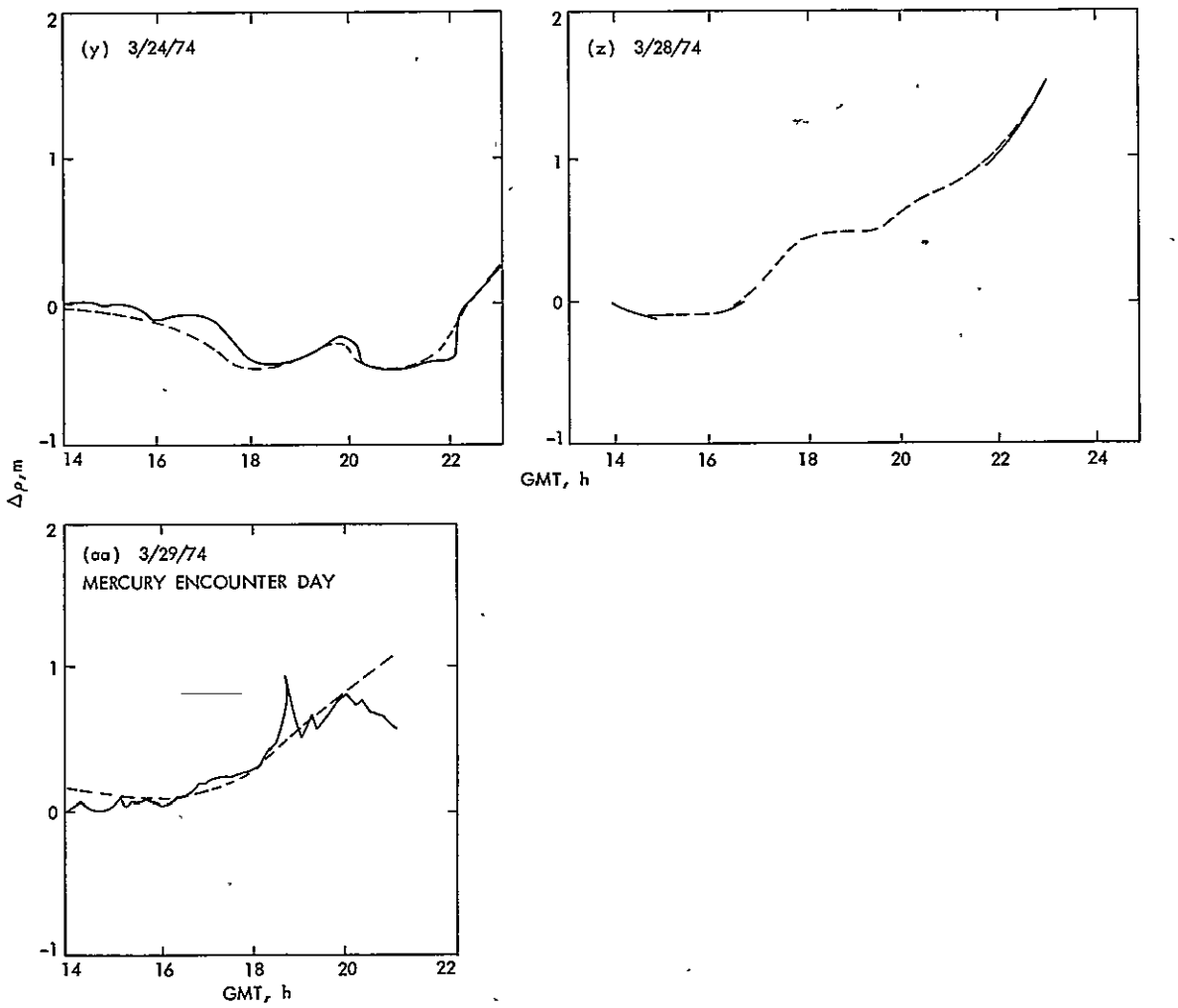

Figure 4-2. S/X Dual Doppler and Faraday Polarization Data Comparisons (Continuation 5)

Besides the gross structure of the S/X dual Doppler, which contains the charged-particle information, the dual Doppler shows a high-frequency noise. An examination of the high-frequency data noise of the December 15, 1973, pass reveals the resolution of the dual Doppler calibration techniques (Fig. 4-3). Figure 4-3 plots about a 1-h segment of the S/X Doppler data. The plot provides a high-resolution view of these data. The S/X dual Doppler was acquired at a rate of one point per minute. A parabola was fit to the data shown. The detrended residuals produced by the fit have a standard deviation of 0.76 cm. Thus, the S/X data of Day 349 have near-centimeter resolution. This is the anticipated noise level.

When the MVM'73 Navigation Team used the tracking data (Doppler and range from DSS 14, DSS 43, and DSS 63) that was acquired in the 9 days following trajectory correction maneuver 3 (March 16, 1974), the estimates of the Mercury encounter coordinates scattered over 200 km. Valid predictions of the encounter coordinates were obtained by rejecting much of the plasma-affected Doppler data. This "predicted" position is shown in Fig. 4-4, along with the actual position known to be "true" from Mercury flyby data.

When the DSS 12 and DSS 14 Doppler tracking data were used to estimate the MVM'73 encounter coordinates with and without Faraday calibrations, it was found that the calibrations reduced the error of the estimates by ∿60% (∿110 km displacement) (Fig. 4-4). When DSS 14 data were used to estimate the encounter coordinates with and without S/X dual Doppler calibrations, it was found that the calibrations reduced the error of the estimates by ∿80% (Fig. 4-5). These two solutions did not support Mercury approach navigation--they were arrived at after Mercury encounter as a demonstration of navigation capability improvements.

Another estimate of the encounter coordinates was made with a combination of the Faraday and S/X dual Doppler calibrations. If S/X dual Doppler existed for a pass, it was used. If it was not available, the Faraday calibrations were used. The improvement realized by the joint use of the two calibration types is ∿80% (180-km displacement) (Fig. 4-6).

Charged-particle calibrations used in this data arc reduction, and in other data arc reductions (Refs. 4-3 through 4-6), have consistently decreased the error of the encounter position estimates.

As the sun-earth-probe angle (SEP) decreased, S/X calibrations indicated dramatic increases in plasma dynamics. Simultaneously, the noises of the S and X Dopplers and the S/X calibrations increased by two orders of magnitude as the SEP decreased from 30 to 3 deg. When these calibrations were used to support MVM'73 navigation, unreasonable results were obtained (Ref. 4-6).

From Fig. 4-7, it can be seen that the noise on the S/X calibration increases rapidly as SEP decreases. Figures 4-8, 4-9, and 4-10 display the unedited S- and X-band Doppler residuals after the removal of the effects of the spacecraft trajectory and earth's troposphere.

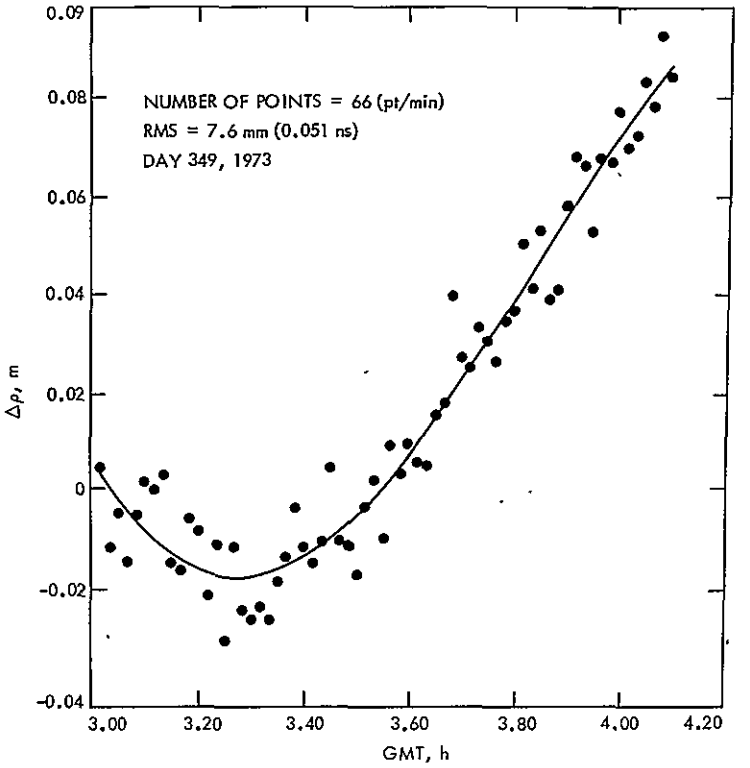

Figure 4-3. High-Frequency S/X Dual Doppler Noise

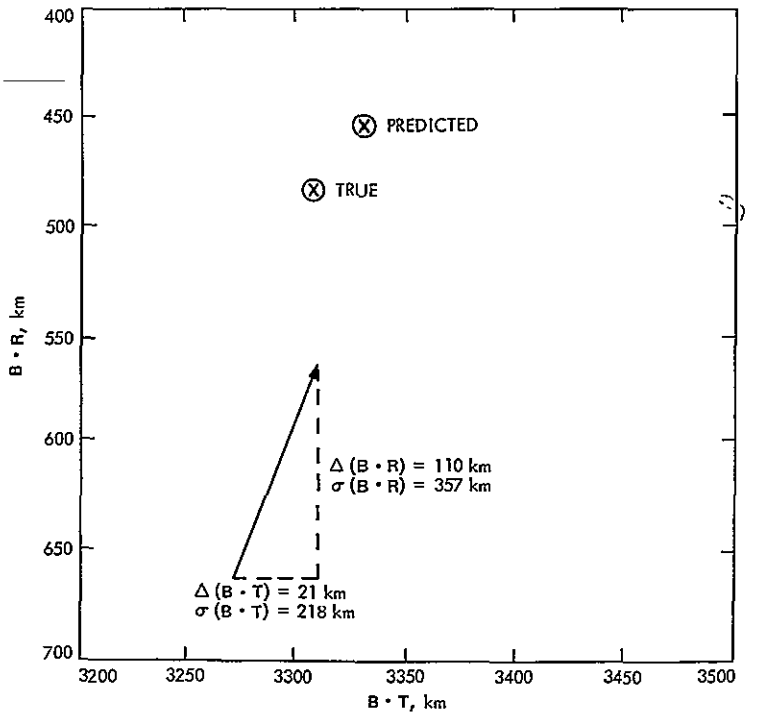

Figure 4-4. MVM'73 Mercury Encounter Plane Coordinate Estimates; Impact of Faraday Calibrations

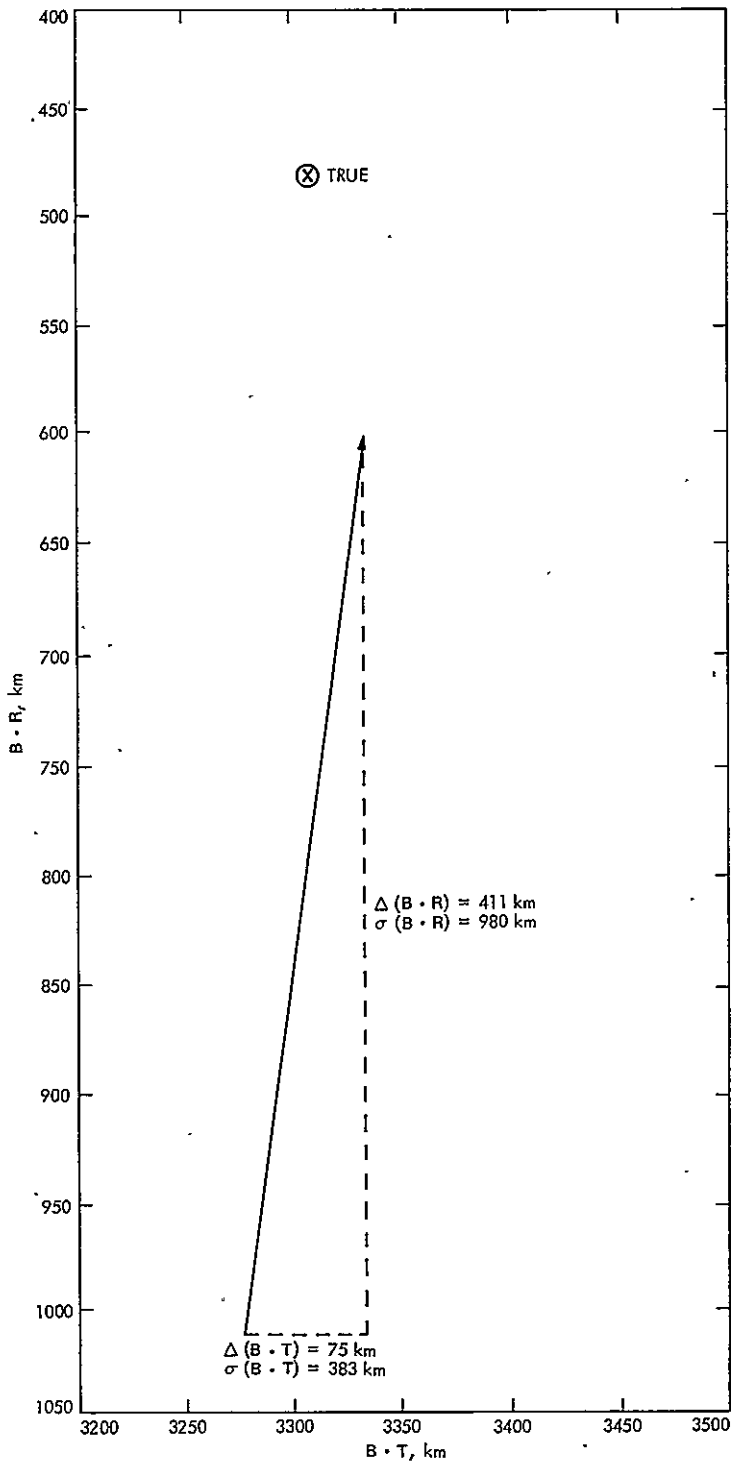

Figure 4-5. MVM'73 Mercury Encounter Plane Coordinate Estimates: Impact of S/X Dual Doppler Calibrations

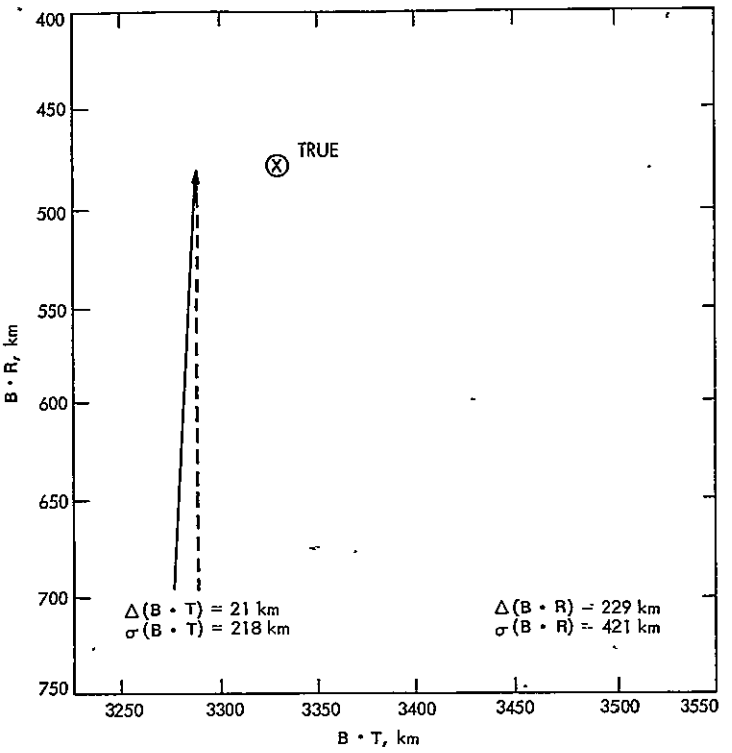

Figure 4-6. MVM'73 Mercury Encounter Plane Coordinate Estimates: Impact of Charged-Particle Calibrations

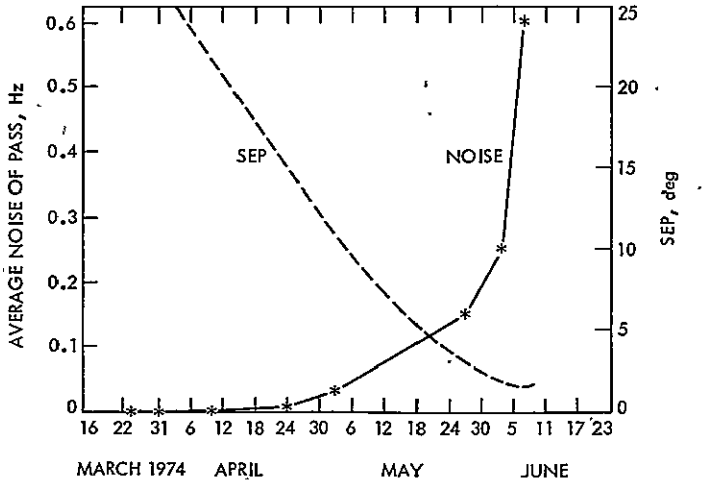

Figure 4-7. Noise in S/X Doppler Calibration vs SEP Angle

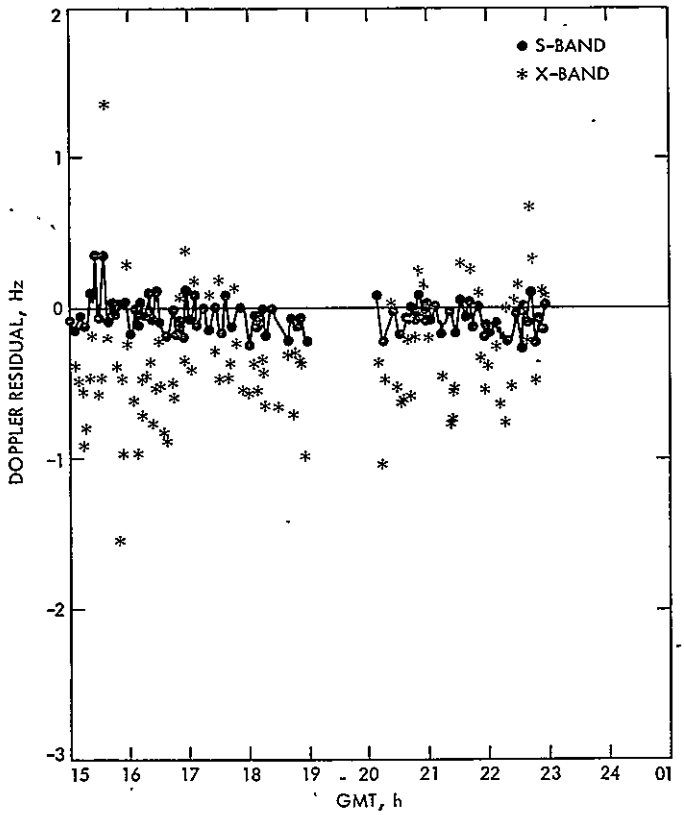

Figure 4-8. S- and X-Band Doppler Residuals for May 27, 1974

Figure 4-11 shows the ratio of the noise of the X-band to that of the S-band residuals. Again these ratios have been obtained by 20-point running averages. For significant fractions of these passes, the ratios of the rms noises are larger than four. This is an important observation. The S/X experiment, as configured for MVM'73, has only an S-band uplink capability. The X-band downlink retransmitted by the spacecraft is obtained by multiplying the S-band uplink by 880/221 (a factor of 3.67). The charged-particle effect on the X-band is approximately 1/16 that of the S-band. Consequently, even if there is no charged-particle effect on the S-band downlink signal, the ratios as computed should be at most 3.67. In other words, considering only plasma-induced noise, the relative rms noise of the X- and S-band Dopplers transmitted from the spacecraft is 3.67 to 1, and, if the downlink S-band Doppler is further scintillated by plasma dynamics, the ratio decreases. Thus, it is obvious that the high-frequency variations of the Dopplers are not due to charged-particle content in the downlink. The most likely explanations are that the phase noise in the X-band received signal exceeds $\pi/2$, so that the ground receiver cannot accurately track the phase of the received X-band signal and that the software did not have the capability to eliminate bad data (Ref. 4-7).

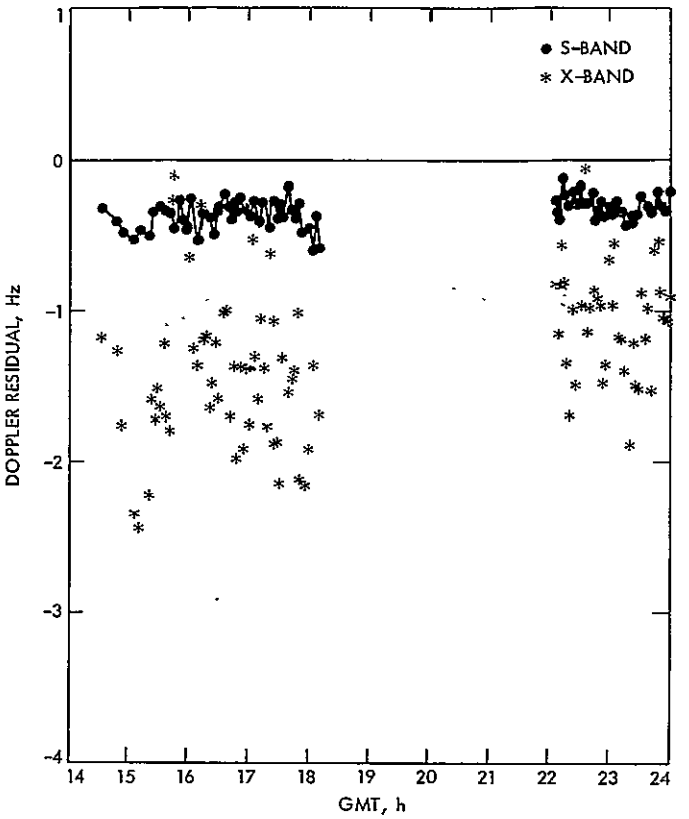

Figure 4-9. S- and X-Band Doppler Residuals for June 3, 1974

This type of problem will be averted in Voyager by going to a one-way transmission using an ultrastable oscillator.

B. RADIO SCIENCE RESULTS

A Radio Science and Celestial Mechanics Team was appointed by the National Aeronautics and Space Administration to conduct radio science experiments with the MVM'73 spacecraft consisting of scientists from JPL, Stanford Univeristy, and the Massachusetts Institute of Technology (see Acknowledgement). Since the celestial mechanics results are not germane to this report, they will not be discussed.

C. VENUS ENCOUNTER

As MVM flew by Venus on its way to Mercury on February 5, 1974, dual-frequency transmissions from the spacecraft were received on earth. These transmissions have been used to refine and increase our knowledge of the planet's environment (Refs. 2-1, 4-8).

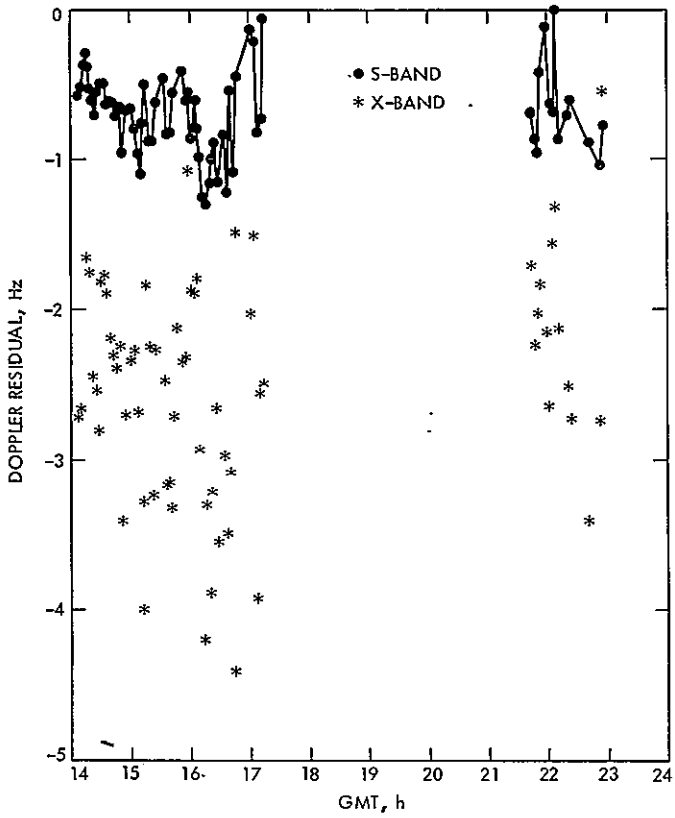

Figure 4-10. S- and X-Band Doppler Residuals for June 7, 1974

D. ATMOSPHERE

Information on Venus' atmosphere was deduced from analysis of the radio signals during occultation. Figure 4-12 is a Mercator projection of a portion of Venus' surface with the ground track and occultation points shown. The dashed portion of the ground track indicates the period of occultation during which no Doppler tracking data were available. Occultation immersion at an altitude of 65 km occurred on the night side at 0.9°N, 69.5°E, with a solar zenith angle of 117.6 deg. Emersion took place on the day side, with a solar zenith angle of 67.1 deg at 56.3°S, 236.4°E. All latitudes and longitudes correspond to the International Astronomical Union convention. During occultation, the spacecraft high-gain antenna was steered in a tear-drop-shaped pattern to track the southern limb of Venus. Because of the shallowness of the occultation, the maximum bending angle of the radio ray was 12.6 deg, corresponding to about the 40-km level in the atmosphere of Venus.

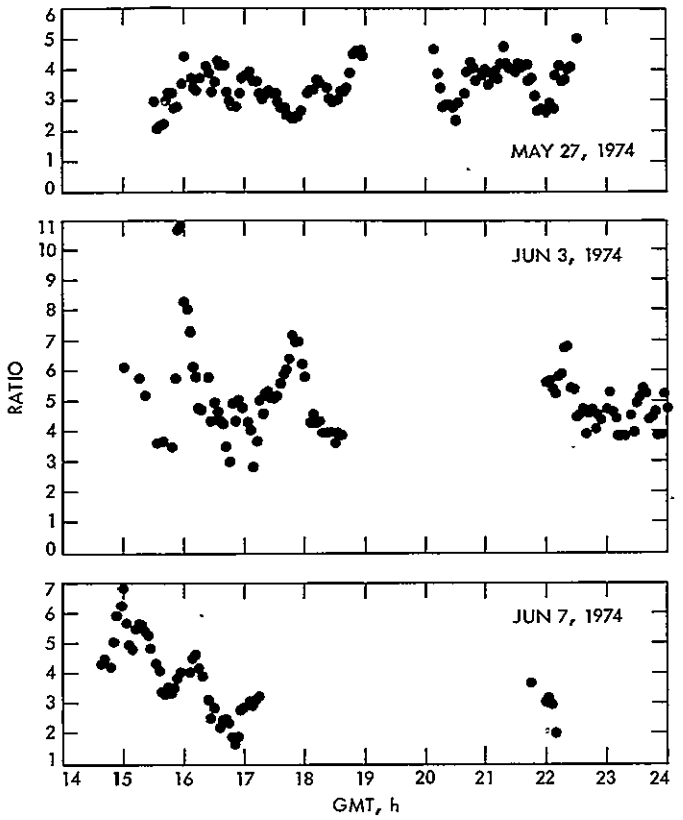

Figure 4-11. Ratio of X-Band to S-Band Doppler Residual Noise

During the flight of MVM'73 to Venus, a study of the spacecraft auxiliary oscillator revealed that its stability was less than adequate for radio science purposes. The entrance into occultation was therefore performed in the two-way mode, with DSS 14 transmitting to the spacecraft, which then coherently retransmitted the received frequency to earth, where it was received by both DSS 14 and DSS 12. Thus, useful measurements of the atmosphere of Venus extend to the point at which the Mariner 10 receiver lost uplink lock, at which point the radio system switched to the auxiliary oscillator for its frequency reference. All subsequent frequency data, including those obtained during the exit from occultation, were perturbed not only by short-time instabilities in the oscillator but also by a long-term drift having a time constant of more than 30 min. Amplitude and differential frequency data were not affected by this problem.

Data were obtained from the closed-loop, phase-locked receivers in the form of nondestructively counted Doppler data and from the open-loop receivers in the form of analog recordings of a frequency-translated signal at S- and X-bands. Substantial amounts of closed-loop data

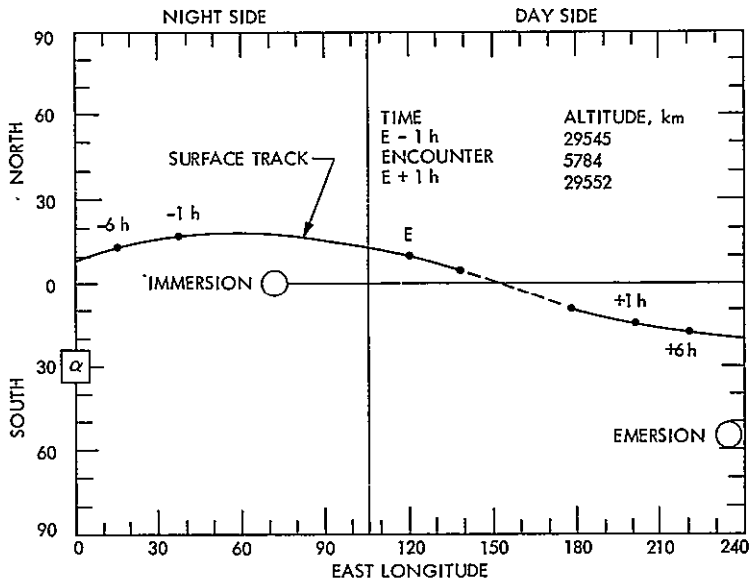

Figure 4-12. Venus Surface Track of Mariner 10

were obtained. The open-loop recordings contain all S- and X-band open-loop data redundantly recorded throughout the duration of the occultation.

Details of the processing of radio occultation data have been described previously (Ref. 4-9). The Doppler data are differenced, in this case at intervals of 1 s, to obtain the Doppler frequency, which is then subtracted from predictions computed on the basis of a precisely determined orbit of the spacecraft to obtain Doppler residuals. After removing bias and drift components, these residuals were then used, along with geometric quantities obtained from a precisely known trajectory of the probe, to obtain a profile of refractivity in the atmosphere of Venus as a function of radius by means of the Abel integral transform. Given the gaseous composition of the atmosphere, which in turn provides the mean molecular weight and the specific refractivity of the gas mixture, one can convert the refractivity into mass or number density. The hydrostatic equation is then used to integrate the density from the top of the sensible atmosphere to obtain the atmospheric pressure at any height, which can be used to determine the temperature by applying the perfect gas law.

A set of temperature profiles determined by such analysis from the S-band data obtained from DSS 14 is shown in Fig. 4-13. For simplicity, the composition was assumed to be 100% carbon dioxide. For the integration of the hydrostatic equation, it is necessary to assume the initial conditions. Three profiles, with initial temperatures corresponding to 150, 200, and 250 K, respectively, are shown. Although there is some divergence in the temperature profiles at the upper levels, all converged to a single profile below a radius of about 6120 km. The altitude scale on the right side of Fig. 4-13 is based

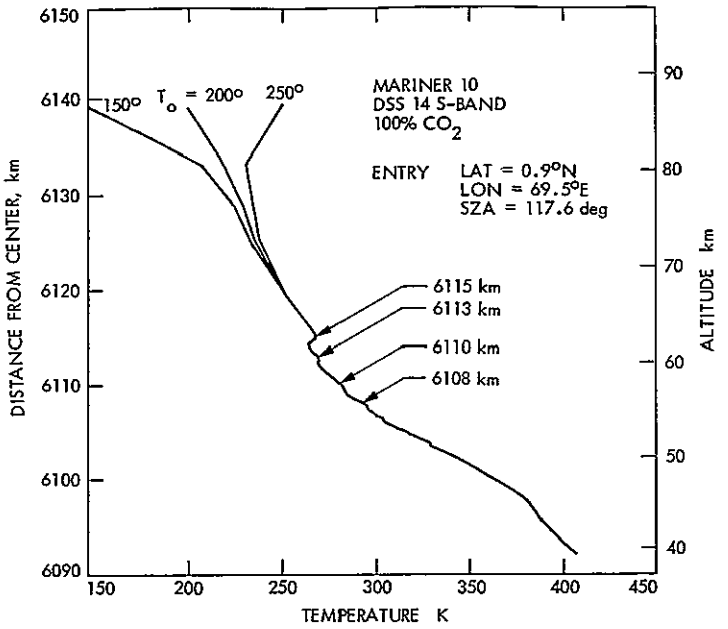

Figure 4-13. DSS 14 Data Venus Temperature Profiles

on a planet radius of 6052 km, which was determined from computations based on radar data (Refs. 4-10, 4-11) and on a combination of radar and Mariner Venus 1967 (MV'67) tracking data (Refs. 4-12, 4-13).

The temperature profile, although obtained at a different latitude and solar zenith angle, is, in general, quite similar to those obtained from the MV'67 radio occultation experiments (Refs. 2-3, 4-14, 4-15). This profile, determined only from the closed-loop data, extends down to a radius of 6092 km, compared to about 6085 km for the profiles from MV'67. The geometry of the MVM'73 encounter was such that the ray path could not penetrate below the 40-km level.

The most striking features of this temperature profile are the four distinct inversions occurring at radii of 6115, 6113, 6110, and 6108 km, as marked by the arrows in Fig. 4-13. These features are thought to be associated with dynamics and cloud structure in the atmosphere of Venus. The top inversion, at 6115 km, could mark the transition between the stable atmosphere above and the convective layers below.

A temperature profile obtained from S-band data received at DSS 12 is shown in Fig. 4-14. Here only one initial temperature of 200 K was used, and the composition was again assumed to be 100% carbon dioxide. This profile, obtained from data independent of those for Fig. 4-13, shows exactly the same features. In particular, the temperature inversions are observed at precisely the same altitudes and have the same magnitudes. In fact, when the profiles are overlaid, they

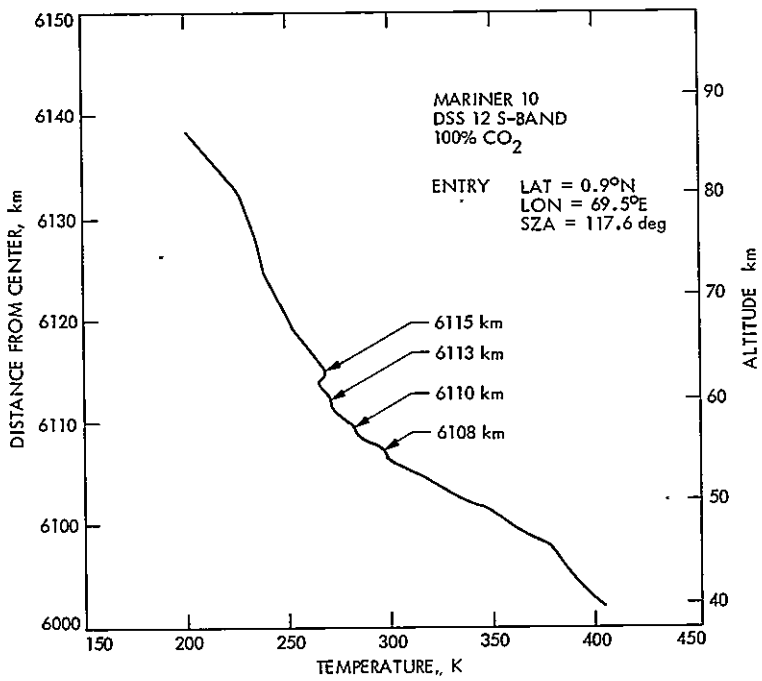

Figure 4-14. DSS 12 Data Venus Temperature Profiles

match exactly, with the exception of a few points at the highest altitudes and some minor roughness in the DSS 14 data below 6105 km caused by counter errors.

The average temperature lapse rate in Figs. 4-13 and 4-14 between the radii of 6106 and 6098 km is about 9.0 K/km, which is very close to the dry adiabatic lapse rate for a carbon dioxide atmosphere. However, at 6098 km, the lapse rate abruptly changes to a somewhat lower value. This change in lapse rate is believed to correspond to the top of the cloud layer proposed by Fjeldbo et al. on the basis of MV'67 radio occultation data (Ref. 4-14). By processing of the open-loop data, it was possible to track the spacecraft through the entire occultation at S-band (Ref. 4-15).

E. NIGHT-SIDE IONOSPHERE

The differential dispersive Doppler frequency perturbations imposed on the MVM'73 radio tracking links by the ionosphere of Venus were utilized to study the vertical electron density distribution in the regions probed by the signals. This was done by inverting the integral equation relating the electron density distribution to the observed Doppler frequency variations. (Detailed discussions of applicable inversion algorithms are available in earlier publications. See, for example, Ref. 4-14.)

Figure 4-15 shows the electron density profile computed from the ingress data. In deriving the ionization, it was assumed that the density distribution was spherically symmetric in the regions probed by the links. A small differential dispersive Doppler shift produced by changes in the electron content of the terrestrial ionosphere (the integrated electron number density along the propagation path through the earth's ionosphere) was removed prior to inverting the data.[1]

In addition, the effect of changes in the interplanetary electron content was approximated by subtracting a linear frequency term from the differential dispersive Doppler data. This frequency drift term was determined by fitting a straight line in a least-squares sense to the Doppler data obtained above the ionosphere of Venus.

As shown in Fig. 4-15, the night side of Venus has two sharp ionization layers. The top layer is located near 142 km altitude (assuming a radius at the solid surface of 6050 km), and it has a peak density of 9×10^3 el/cm^3. A second peak with a density of 7×10^3 cm^{-3} was observed at 124 km altitude. Above 170 km, the density appears to

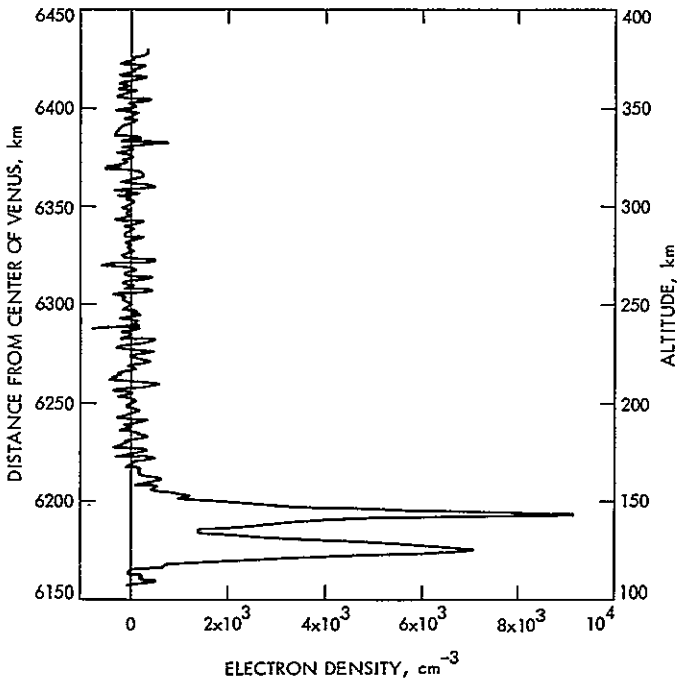

Figure 4-15. Venus Ingress Electron Density

[1]The electron content of the earth's ionosphere was obtained by measuring the Faraday rotation of a signal transmitted from ATS 1 to Goldstone during the occultation experiment. The content data were later corrected for the different path from MVM'73 employing a method described by von Roos et al. (Ref. 4-16).

be less than 200 cm^{-3}. The sharpness of the night-side layers indicates that the ions in this region are heavy and cold. The topside plasma scale height was only on the order of 4 km. By comparison, the diameter of the first S-band Fresnel zone--which is a convenient measure of the altitude resolution provided by the radio data--was about 2 km. An expanded view of the nighttime layers is presented in Fig. 4-16.

F. DAY-SIDE IONOSPHERE

The egress measurements made with MV'67 on the day side of Venus were also affected by multipath propagation at the lower frequencies; and the accuracy of the S-band data was limited by the stability of the crystal oscillator employed to generate the tracking signal from the spacecraft (Ref. 4-17). MVM'73 has, therefore, provided us with the most accurate measurements to date of the day-side ionosphere of Venus. The new results are shown in Figs. 4-17 and 4-18.

As illustrated by Fig. 4-17, the computed electron density profile shows a minor layer near 128 km altitude. The main layer has a peak density of 2.9×10^5 el/cm^3 at 142 km altitude. The ions in this region are probably formed through photoionization of CO_2 by extreme solar ultraviolet. Assuming that the slant optical depth in the extreme ultraviolet is equal to one at the ionization peak yields a CO_2 density on the order of 2×10^{10} cm^{-3} at this atmospheric level. The plasma scale height in the 145- to 160-km altitude region is approximately 18 km, indicating a temperature on the order of 400 K. Similar

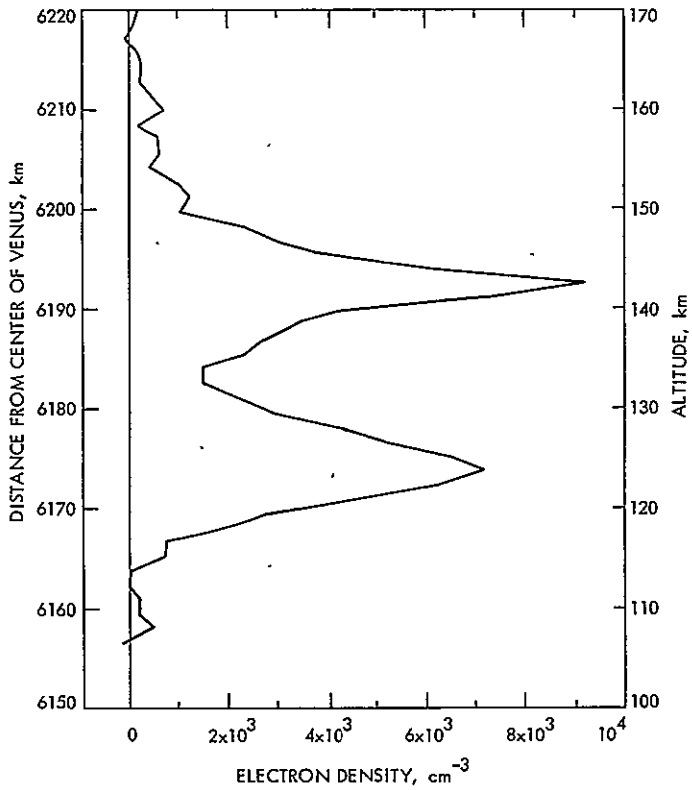

Figure 4-16. Expanded View of Venus Ingress Electron Density

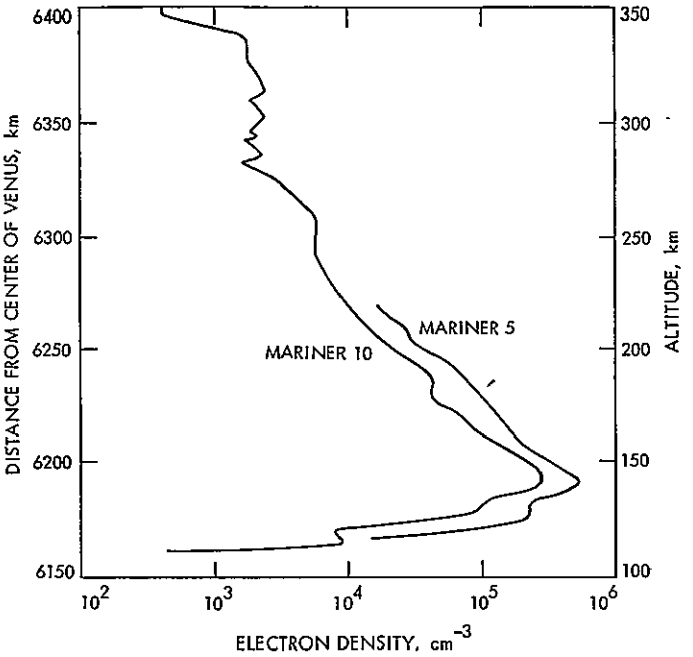

Figure 4-17. Electron Densities Obtained from the Day-Side Ionosphere of Venus by MV'67 and MVM'73

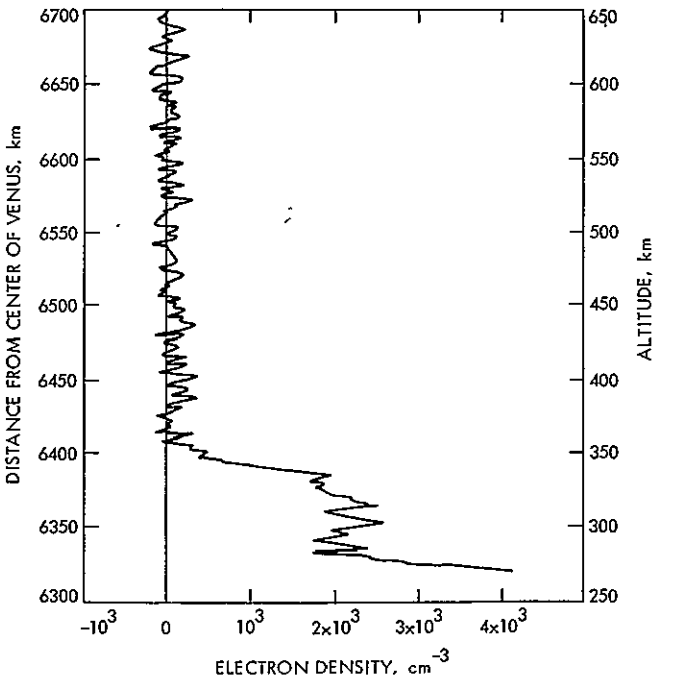

Figure 4-18. Venus Ionospheric Topside Electron Density

temperatures were reported by the Ultraviolet Experiment Team (Ref. 4-18) for the exosphere of Venus. A marked increase in the plasma scale height with altitude may reflect transitions to lighter ions or an increasing plasma temperature.

The topside measurements illustrated in Fig. 4-18 show an abrupt drop in the electron density from about 2000 cm^{-3} at 335 km altitude to less than 200 cm^{-3} at 360 km. This is probably the ionopause boundary. The measurements between 280 and 335 km altitude show a density of about 2000 el/cm^3. The noisy appearance of the profile in this altitude region suggests turbulence. Earlier measurements with MV'67 indicated that on October 19, 1967, the ionopause was located near 500 km altitude. The region below the ionopause boundary appeared to consist of turbulent plasma with a density on the order of 10^4 el/cm^3. The differences between the MV'67 and MVM'73 results may be due to changes in solar activity. Ground-based observations of the 10-cm solar radio emission yielded values of 120×10^{-22} and 76×10^{-22} W/m^2 Hz at the time of the Mariner 1967 and 1973 encounters, respectively.

Between the ionization peak and 335 km altitude, the electron density drops off by a factor of 1.5×10^2--which is equivalent to 5 plasma scale heights. This result, together with the atmospheric density calculated at 142 km altitude (2×10^{10} cm^{-3}), may be utilized to estimate the neutral gas density near the ionopause. For instance, by assuming that the plasma scale height between 142 and 335 km is twice as large as the neutral scale height, one finds a neutral gas density on the order of 10^6 cm^{-3} at 335 km altitude. A recent model developed by Kumar and Hunten (Ref. 4-19) shows that He may be the principal constituent near the ionopause boundary.

A number of models have been proposed to explain the interaction between the solar wind and the atmosphere of Venus (Refs. 4-20 through 4-25). The new improved measurements at the ionopause boundary might help resolve some of the remaining uncertainties in these model studies.

G. ERROR SOURCES

The exact ratio between the X-band (f_X) and S-band (f_S) downlink frequencies transmitted from MVM'73 was 11/3. By utilizing the differential dispersive Doppler shift ($f_S - 3 f_X/11$) in our analysis, frequency variations due to oscillator instabilities, phase jitter in the transmitted signals, motion of the spacecraft and the tracking station, and phase scintillations in the terrestrial troposphere were prevented from producing errors in the computed ionization profiles.

The frequency variations seen in the differential dispersive Doppler data consist of the refractive signature of the ionosphere of Venus--which is the effect to be studied--plus noise produced by phase scintillations in the interplanetary medium and the terrestrial ionosphere, and by differential system phase jitter. The effects of the interplanetary medium and the terrestrial ionosphere were removed in an approximate manner, as described earlier. An analysis of the errors produced by the differential system phase jitter is presented.

The signal level in the input waveguide to the S-band maser amplifier was -128.0 dBm (i.e, 128 dB below the 1-mW level) during the ionospheric measurements. The noise temperature of the S-band system was 13.4 K. The corresponding values for the X-band receiver system were -135.5 dBm and 21.5 K. The S-band system noise was not correlated with the X-band noise. Thus, the system noise in the two receiver channels produced phase jitter in the differential Doppler data. The resulting noise in the computed ionization profiles consisted of random density variations with a zero mean. A formal error analysis using an altitude filter width of 1 km yields a standard deviation on the order of 2×10^2 el/cm^3. However, one should keep in mind that systematic errors, due to nonlinear changes in the Doppler shift produced by the interplanetary medium, might have caused errors larger than 2×10^2 cm^{-3}. The only way one can completely eliminate the latter error source is to simultaneously conduct dual-frequency propagation measurements between two planetary spacecraft and the tracking station. While one spacecraft is being used to probe the planetary ionosphere, the other can monitor changes in the interplanetary medium and the terrestrial ionosphere and thereby provide a zero calibration for the planetary measurements. An experiment of this type was executed on the Viking dual-orbiter mission to Mars.

H. TURBULENCE OBSERVATIONS OF THE ATMOSPHERE OF THE PLANET VENUS

Using the single-frequency S-band scintillation spectrum of MV'67, Woo, Ishimaru, and Kendall (Ref. 4-26) found turbulence to be strongest at an altitude of approximately 60 km, and an outer scale size L_o maximum turbulence dimension of 100 m. The original results were obtained under the assumption that L_o was much smaller than the Fresnel size. This restriction has now been removed from the analysis, and it has been shown that the frequency dependence changes significantly with L_o. This property makes the dual-frequency experiment an extremely valuable tool for studying the characteristics of the turbulence (Ref. 4-27).

Figure 4-19 shows the MVM'73 flyby turbulence configuration, which is the distance between the spacecraft and the Venus atmosphere, and v free spacecraft velocity transverse to the line-of-sight path. The turbulence is assumed to be concentrated in a spherical layer, with the extent of the turbulence in the X-Z phase characterized by a and that in the y direction by b. Shown in Fig. 4-20 is the time history of the MVM S-band entrance occultation signal level, where B_L is the one-sided loop noise bandwidth of the digital phase-locked loop, r the time constant of the amplitude estimating circuit, and h the sampling period. It should be pointed out that a long time constant was used in Fig. 4-20 to expose the gross features in the signal variation.

Two regions of turbulence were identified at altitudes of 45 and 60 km. The analysis of the region from approximately 55 to 70 km indicated that X-band turbulence-induced fluctuations were larger than those at S-band. The values of a = 220 km, b = 4 km, and $L_o > 5$ km were obtained, indicating that the outer scale of turbulence is as large as the vertical extent of the region of strong turbulence.

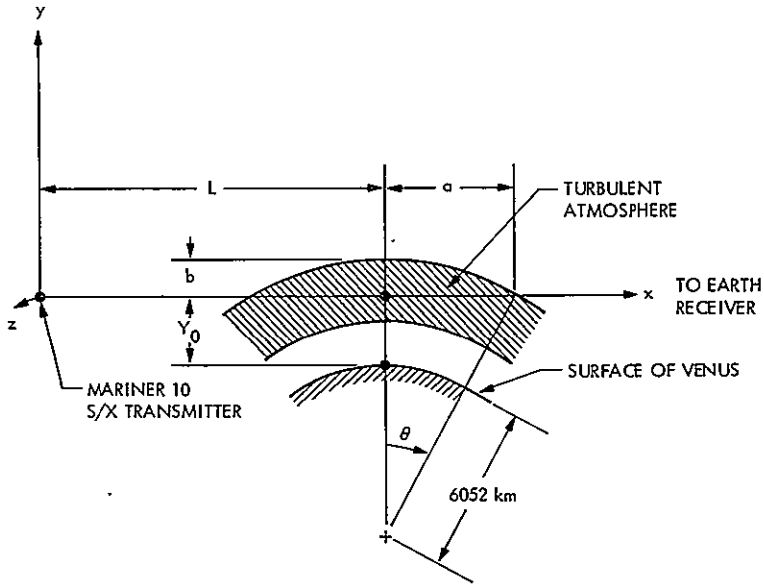

Figure 4-19. MVM'73 Venus Turbulence Occultation Configuration

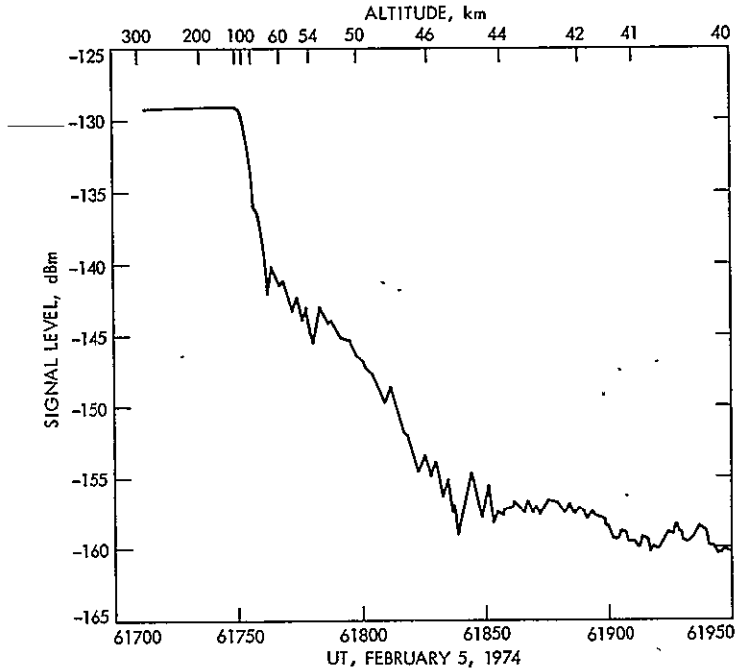

Figure 4-20. S-Band Signal Level vs Time for Occultation Entrance

I. MVM'73 MERCURY ENCOUNTER

The MVM'73 spacecraft's first encounter with Mercury took place on March 29, 1974 (Ref. 4-28). Closest approach occurred approximately 700 km above the surface on the dark side of the planet. About 77 s past periapsis passage, the spacecraft was occulted by Mercury. During ingress, the coherently related S- and X-band radio tracking links were employed to search for a night-side atmosphere near 1.1°N latitude. Measurements were also made during egress, which occurred on the day side of Mercury near 67.6°N latitude. The distances between the spacecraft and the planetary limb were approximately 2150 and 8380 km at the time of ingress and egress, respectively. The transverse velocity component of the radio beams orthogonal to the limb was about 5 km/s during the measurements.

In searching the radio recordings for evidence of an atmosphere on Mercury, evidence of dispersive and nondispersive Doppler effects in the data was sought. However, the main part of the effort was devoted to the analysis of the dispersive Doppler shift because this is the most sensitive measure of atmospheric gas which can be obtained from the occultation recordings. As an example, it takes more than 10^{17} He atoms/cm^3 near the surface of Mercury to produce a detectable nondispersive frequency shift. However, if 1 out of every 1000 He atoms is ionized (forming $He^+ + e$ ion pairs), it is necessary to have only on the order of 3×10^6 He atoms/cm^3 to produce a detectable dispersive atmospheric Doppler shift (Ref. 4-29). The dispersive frequency data provide a sensitive measure of changes in the electron density along the tracking link. The differential dispersive Doppler data may be utilized to determine the vertical electron density distribution in the atmosphere of Mercury. This task can be accomplished by inverting the integral equation relating the electron density distribution to the observed frequency fluctuations (Ref. 4-30). The resulting ionization profiles are displayed in Fig. 4-21.

Prior to the inversion of the Doppler data, the frequency perturbations produced by the terrestrial ionosphere and the interplanetary medium were removed in an approximate manner. The terrestrial frequency shift was produced by changes in the average electron density along the propagation path through the earth's ionosphere. This effect was determined by measuring the Faraday rotation of a signal transmitted from ATS 1 to Goldstone during the occultation measurements. Later the Faraday results were corrected for the different signal path from MVM by utilizing a method described by von Roos (Ref. 4-17). The correction due to electron density changes in the interplanetary medium was approximated by subtracting a linear frequency term from the dispersive Doppler data. This frequency correction term was determined by fitting a straight line in a least-squares sense to Doppler data obtained above 400 km altitude.

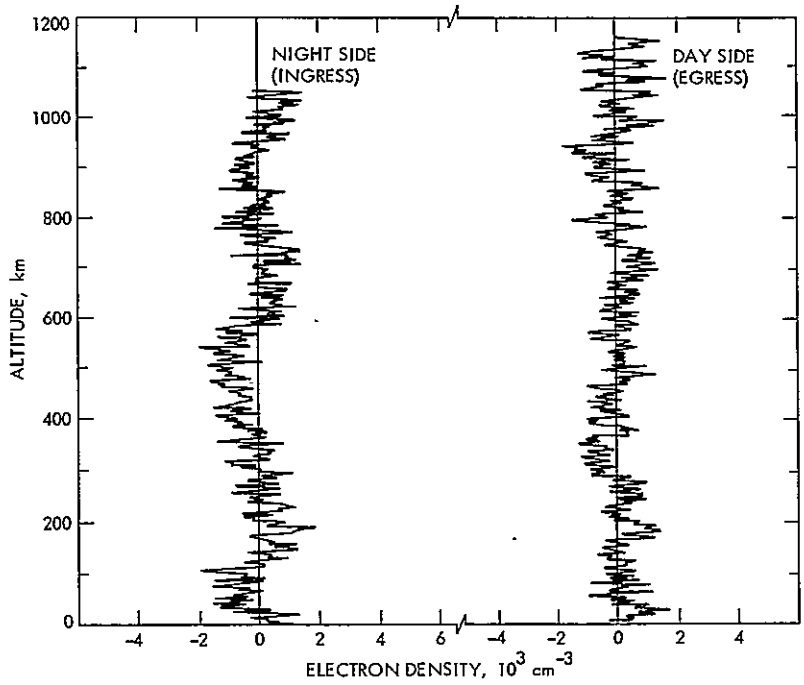

Figure 4-21. Mercury Electron Density Profiles

During ingress, the night side of Mercury was probed near 1.1°N latitude and 67.4°E longitude (planetocentric coordinates based on IAU conventions). The solar zenith angle in this region was approximately 167 deg. The resulting electron density profile is shown on the left side of Fig. 4-21. No clear signature of a nighttime ionosphere was observed---which is not surprising considering the fact that this region of Mercury had been out of direct sunlight for about 38 terrestrial days.

The S- and X-band downlink carrier frequencies were, during ingress, coherently derived from a 2.1-GHz uplink carrier signal. The uplink carrier was in turn generated with a station rubidium vapor reference oscillator. During the 16.5-min round-trip (station-spacecraft-station) propagation time, the earth moved about 0.25 mrad as observed in a Mercury-centered inertial frame of reference. This motion caused the uplink to intercept the planetary limb before the downlinks. The altitude separation between the uplink and the downlinks was approximately 0.5 km. Zero altitude in the ingress profile was determined from the phase diffraction effects observed at the tracking station approximately 8-1/4 min after the uplink grazed the surface of Mercury. Using the time of the observed diffraction effects and the best ephemerides available for MVM and Mercury, one finds that the radius of the planetary surface was 2439.5 km at the ingress point.

As MVM moved in behind Mercury, the 2.1-GHz uplink carrier signal became progressively weaker, and this caused the spacecraft's phase-locked-loop receiver to go out of lock. An onboard crystal oscillator was automatically switched in to provide the reference frequency for

the downlinks when loss of lock occurred. This operating mode is commonly referred to as one-way tracking.

Figure 4-22 shows the downlink diffraction patterns observed at Deep Space Station 14 as the spacecraft emerged from occultation in the one-way mode. By utilizing the time of egress, together with data on the ephemerides of MVM and Mercury, we obtain a value of 2439 km for the planetary radius at the egress point.

The dispersive Doppler data obtained during egress yielded the ionization profile shown on the right-hand side of Fig. 4-21. These measurements were made on the day side of Mercury near 258.4°E longitude and 67.6°N latitude. The solar zenith angle in this region was 67.6 deg. The day-side electron density was too low to be detectable. The level of the computer electron density noise was in this particular experiment set by phase scintillations due to spatial and temporal variations in the electron density in the terrestrial ionosphere and the interplanetary medium.

The dispersive frequency measurements yielded an upper limit to the day-side electron density of 10^3 cm^{-3}. This observation may be used, together with information on the interaction between the solar wind and the atmosphere, to infer an upper limit to the neutral gas density.

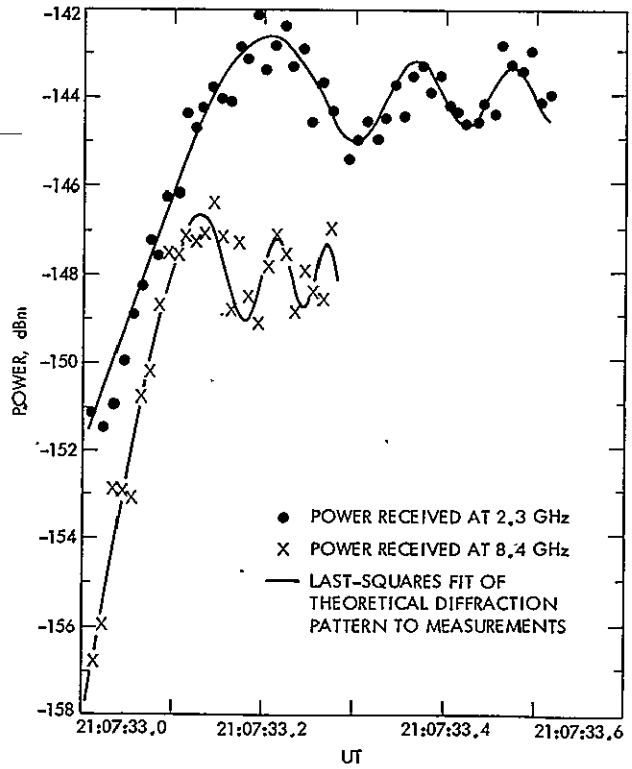

Figure 4-22. S- and X-Band Mercury Diffraction Effects

As an example, if an analogy with the day side of Venus is applicable, one finds that the atmospheric density near the surface of Mercury should not exceed the density found near the ionopause boundary of Venus; i.e., 10^6 molecules/cm^3 (Ref. 4-31)--otherwise one would have detected ionization on Mercury too. Assuming an atmospheric temperature of 500 K, this result yields an upper limit to Mercury's surface pressure of 0.7×10^{-10} mb.

The upper limit to the surface number density reported here appears to be consistent with other MVM'73 data. For instance, the television pictures of Mercury's surface show no evidence of any atmospheric erosion of the ancient land areas, making it unlikely that the planet has possessed any tangible atmosphere since the end of the heavy bombardment by small planetesimals (Ref. 4-32). Furthermore, the ultraviolet spectrometer experiment detected only a small amount of helium, corresponding to a partial pressure of about 0.5×10^{-11} mb near the terminator (Ref. 4-33). Based on these UV measurements, Hartel et al. (Ref. 4-34) have developed a global model for Mercury's helium exosphere which shows that the gas density near the egress point may be less than 10^4cm^{-3}.

J. SOLAR CORONA MEASUREMENTS

As the MVM spacecraft moved toward superior conjunction, the line-of-sight passed through the solar corona. The ranging at X- and S-band offered an opportunity to measure the differential group velocity delay, which is proportional to the total electron content along the line-of-sight. H. T. Howard has reduced the data (Ref. 4-35), and it is illustrated in Fig. 3-4. The final interpretation of these delay measurements is now under way.

K. SCINTILLATION MEASUREMENTS OF THE SOLAR CORONA

A great deal of information on the structure of density fluctuations in the solar wind has been obtained in recent years through direct spacecraft measurements as well as indirect scintillation observations of radio sources (Ref. 4-36). Near 1 astronomical unit in situ measurements indicate that the density spectrum is approximately power-law in the spatial wave number range $10^{-8} < \kappa < 10^{-1}$ km^{-1}, with a small enhancement at the wave number corresponding to the proton gyroradius. In regions of the solar wind not yet probed by direct spacecraft, we must rely on scintillation observations. Unfortunately, the results to date have been fragmentary, and some questions remain unsettled (Ref. 4-37).

Intensity scintillations respond only to scale sizes smaller than the first Fresnel zone size because of Fresnel filtering (Ref. 4-38). Thus, these more widely observed scintillations yield information only on the high wave number ($\kappa \gtrsim 10^{-3}$ km^{-1} for decametric wavelengths) portion of the density spectrum. Another observation useful for studying density fluctuations near the sun is spectral broadening of monochromatic spacecraft signals. Woo, et al. (Ref. 4-39) have, however,

shown that these observations, like the intensity scintillations, are useful only for studying small-scale structure ($\kappa \geq 10^{-2}$ km^{-1}).

Probing the full range of scale sizes observed by in situ spacecraft requires the measurement of phase scintillations. With radio stars, this can be achieved with long-baseline interferometry. Unfortunately, Cronyn (Ref. 4-40) has shown that very-long-baseline interferometry (VLBI) observations yield information only on scale sizes smaller than $\sigma/1.5$, where σ is the baseline distance. Thus, even with a baseline of 1 earth radius, only $\kappa \geq 2.3 \times 10^{-4}$ km^{-1} can be studied. In principle, the full potential of phase scintillations can be realized with coherent spacecraft signals. In practice, however, it may be difficult to separate the turbulence-induced fluctuations from those due to uncertainties in the spacecraft trajectory and phase instability of the radio source. Callahan (Ref. 4-41) has employed a group-phase velocity technique called differenced range versus integrated Doppler (DRVID), which is insensitive to trajectory errors. Unfortunately, the DRVID data are very noisy and only frequencies lower than 10^{-3} Hz ($\kappa \lesssim 2 \times 10^{-5}$ km^{-1} have been measured. Both trajectory and radio source frequency drift errors are eliminated in a phase differencing technique recently proposed by Woo (Ref. 4-42) using a dual-frequency phase-coherent system.

L. OBSERVATIONS

The phase data used and discussed are the normal closed-loop two-way navigational data. By taking the difference between the S-band and 3/11 of the X-band phases, we cancel out the common uplink and effectively have a one-way downlink phase difference measurement.

The data presented were obtained on April 29/30, 1974, and May 1, 1974, when the spacecraft was located at an approximate heliocentric celestial latitude of $-4°$ with solar elongation angles $\theta = 12.6$ and 11.5 deg, respectively. During this time, the MVM spacecraft was ~1.6 astronomical units from the sun. For both days, the observation time exceeded 4 h and the sampling rate was 0.1 s^{-1}.

The phase difference spectrum for May 1, 1974, is typical and is shown in Fig. 4-23. The corresponding 90% confidence intervals have been calculated and are indicated on the spectrum. The spectrum covers a frequency range of $10^{-4} \lesssim f \lesssim 5 \times 10^{-2}$ Hz, which corresponds to the spatial wave number range $2 \times 10^{-6} \lesssim \kappa \lesssim 10^{-3}$ km^{-1} if the solar wind velocity is assumed to be 350 km s^{-1}. The straight dashed lines represent approximations. The slopes of the spectra for April 29/30 and May 1 are -2.5 and -2.6, respectively, to the measured spectra.

It was demonstrated that the dual-frequency S/X system can be used to measure phase scintillations in the solar wind. The MVM'73 observations presented in this report probed a wider range of scale sizes (with a corresponding frequency range of 10^{-4} to 5×10^{-1} Hz) than has ever been possible before.

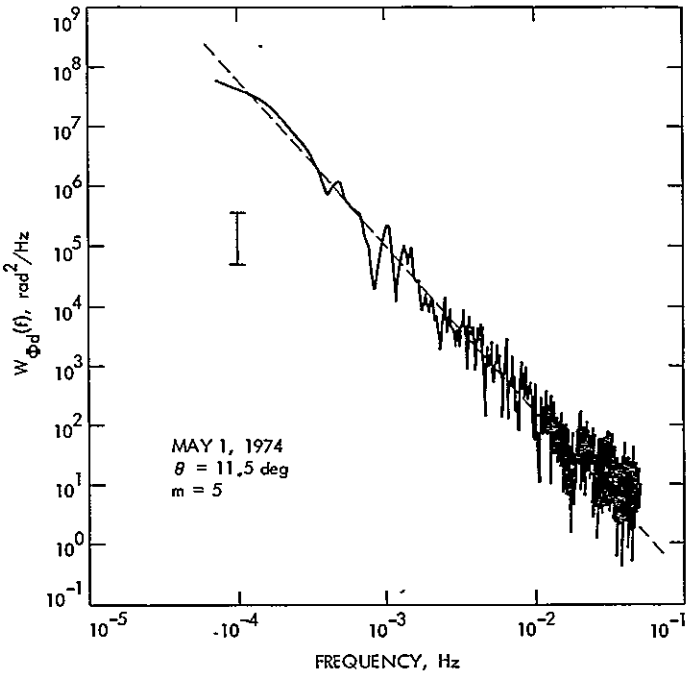

Figure 4-23. S/X-Band Phase Difference Scintillation Spectrum

REFERENCES

2-1. Howard, H.T., Tyler, G.L., Fjeldbo, G., Kliore, A.J., Levy, G.S., Brunn, D.L., Dickinson, R., Edelson, R.E., Martin, W.L., Postal, R.B., Seidel, B., Sesplaukis, T.T., Shirlety, D.L., Stelzried, C.T., Sweetnam, D.N., Zygielbaum, A.I., Esposito, P.B., Anderson, J.D., Shapiro, I.I., and Reasenberg, R.D., Science, Vol. 183, p. 1297, 1974.

2-2. Fjeldbo, G., and Eshleman, V.R., Planet. Space Sci., Vol. 16, p. 1035, 1968.

2-3. Koehler, R.L., J. Geophys. Res., Vol. 73, p. 4884, 1968.

2-4. Mariner Stanford Group, Science, Vol. 158, p. 1678, 1967.

2-5. Brunn, L., and Hanna, C., Celestial Mechanics and Radio Science Experiment, PD 615-11, Jet Propulsion Laboratory, Pasadena, Calif., March 1, 1972 (JPL internal document).

2-6. Mariner Venus Mercury 1973 X-Band Transmitter (XTX) Final Report, Motorola, Scottsdale, Ariz., Dec. 1972.

2-7. XTX SE Design Review, Jet Propulsion Laboratory, Pasadena, Calif., Apr. 4, 1972 (JPL internal document).

2-8. Brunn, L., MVM 73 S/X Test Procedure (Rev. A), IOM 3396-72-302 REVA, Jet Propulsion Laboratory, Pasadena, Calif., Sept. 1972 (JPL internal document).

2-9. Results of Flight 1 RFS/Spare XTX Testing in JPL, IOM 3396-72-387, Jet Propulsion Laboratory, Pasadena, Calif., Nov. 2, 1972 (JPL internal document).

2-10. Brunn, L., and Madsen, B., VM 73 Flight 2 RFS/Flight XTX Test Results, IOM 3396-73-27, Jet Propulsion Laboratory, Pasadena, Calif., Jan. 1973 (JPL internal document).

2-11. Brunn, L., S/X Thermal Vacuum and Ranging Delay Test Results, IOM 3396-73-237, Jet Propulsion Laboratory, Pasadena, Calif., Aug. 1973 (JPL internal document).

2-12. Schnieder, W.A., MVM'73 S/X Band Antenna Development Report, The Boeing Co., Feb. 1973.

2-13. Bathker, D.A., "Dual Dichroic Feed Performance," Avionics Panel Symposium, Munich, Nov. 1973, Agard Conference Preprint #139 29, Neuilly sur Seine, France.

2-14. Clarke, V.C., "117.6 Kilobit Telemetry from Mercury--A Major Deep Space Telecommunication Advance," International Telemetry Conference, Los Angeles, Oct. 1974.

2-15. Evanchuk, V.L., "117.6 Kilobit Telemetry from Mercury--In-Flight Analysis," International Telemetry Conference, Los Angeles, Oct. 1974.

2-16. Clauss, R., and Wiebe, E., "Low-Noise Receivers: Microwave Maser Development," in The Deep Space Network Progress Report, Technical Report 32-1526, Vol. XIX, Jet Propulsion Laboratory, Pasadena, Calif., pp. 93-95, Feb. 15, 1974.

2-17. Clauss, R., Wiebe, E., and Quinn, R., "Low-Noise Receivers: Microwave Maser Development," in The Deep Space Network Progress Report, Technical Report 32-1526, Vol. XI, Jet Propulsion Laboratory, Pasadena, Calif., pp. 71-80, Oct. 15, 1972.

2-18. Donnelly, H., Shallbetter, A.C., and Weller, R.E., "Block IV Receiver-Exciter Development," in JPL Space Programs Summary 37-36, Vol. II, Jet Propulsion Laboratory, Pasadena, Calif., pp. 115-132, Nov. 30, 1965.

2-19. Martin W.L., and Zygielbaum, A.I., Mu-II Ranging, Technical Memorandum 33-768, Jet Propulsion Laboratory, Pasadena, Calif. (in press).

3-1. Evanchuk, V.L., MVM Prime Mission Final Report, IOM 3396-74-122, Jet Propulsion Laboratory, Pasadena, Calif., June 20, 1974 (JPL internal document).

3-2. MVM 1973 Project Final Report, Technical Memorandum 33-734, Vol. I, Jet Propulsion Laboratory, Pasadena, Calif., Dec. 1975.

3-3. Ohlson, J.E., and Reid, M.S., Conical-Scan Tracking With the 64-m-Diameter Antenna at Goldstone, Technical Report 32-1605, Jet Propulsion Laboratory, Pasadena, Calif., Nov. 1975.

3-4. Davis, E.K., and Traxler, M., MVM 73 Final Report, Tracking and Telemetry, Technical Memorandum 33-797, Jet Propulsion Laboratory, Pasadena, Calif. (to be published).

3-5. Howard, H.T., private communication.

3-6. Brunn, L., VM 73 XTX Failure Analysis Study, IOM 3360-74-032, Jet Propulsion Laboratory, Pasadena, Calif., May 22, 1974 (JPL internal document).

4-1. Springett, J.C., Kollar, F.J., Results of the MVM'73 X-Band Telemetry Experiment, 615-149, Jet Propulsion Laboratory, Pasadena, Calif. May 1974 (JPL internal document).

4-2. Winn, F.B., Yip, K.W., and Reinbold, S.J., "DSN-MVM'73 S/X Dual-Frequency Doppler Demonstration," in The Deep Space Network Progress Report 42-22, Jet Propulsion Laboratory, Pasadena, Calif., pp. 28-50, Aug. 15, 1974.

4-3. Kip, K.W., and Mulhall, B.D., "A System Analysis of Error Sources in the Technique Used for Ionospheric Calibration of Deep Space Probe Radio Metric Data," in The Deep Space Network Progress Report, Technical Report 32-1526, Vol. XVII, Jet Propulsion Laboratory, Pasadena, Calif., pp. 48-67, Oct. 15, 1973.

4-4. Winn, F.B., Yip, K.W., and Dysart, B.W., Current MVM'73 Charged Particle Calibration Experience (21 November 1973), IOM 391.3-763, Jet Propulsion Laboratory, Pasadena, Calif., Dec. 5, 1973 (JPL internal document).

4-5. Winn, F.B., and Yip, K.W., Ionospheric Charged Particle Influence on Mercury B-Plane Coordinate Estimates (Report 4--March 16 to March 24, 1974), IOM 391.3-775, Jet Propulsion Laboratory, Pasadena, Calif., Feb. 22, 1974 (JPL internal document).

4-6. Winn, F.B., and Yip, K.W., Actual Corruption of the MVM'73 B-plane Coordinate Estimates: Ionospheric Charged Particle Influences on Goldstone DSN Tracking Data (Report 3—January 21 to February 5, 1974), IOM/391.3-775, Feb. 22, 1974 (JPL internal document).

4-7. Yip, K.W., Winn, F.B., and Reinbold, S.J., "DSN-MVM'73 S/X Dual-Frequency Doppler Demonstration During Superior Conjunction," in The Deep Space Network Progress Report 42-25, Jet Propulsion Laboratory, Pasadena, Calif., pp. 47-55, Feb. 15, 1975.

4-8. Fjeldbo, G., Seidel, B.L., Sweetnam, D., and Howard, T., J. Atmos. Sci., Vol. 32, No. 6, pp. 1232-1236, June 1975.

4-9. Kliore, A.J., Cain, D.L., Fjeldbo, G., Seidel, B.L., Sykes, M. J., and Rasool, S.I., Icarus, Vol. 17, p. 484, 1972.

4-10. Ash, M.E., Campbell, D.B., Dyce, R.B., Ingalls, R.P., Jurgens, R., Pettengill, G.H., Shapiro, I.I., Slade, M.A., Smith, W.B., and Thompson, T.W., Science, Vol. 160, p. 985, 1968.

4-11. Melbourne, W.G., Muhleman, D.O., and O'Handley, D.A., ibid., p. 987.

4-12. Anderson, J.D., Cain, D.L., Efron, L., Goldstein, R.M., Melbourne, W.G., O'Handley, D.A., Pease, G.E., and Tausworthe, R.C., J. Atmos. Sci., Vol. 25, p. 1171, 1968.

4-13. Eshleman, V.R., Fjeldbo, G., Anderson, J.D., Kliore, A., and Dyce, R.B., Science, Vol. 162, p. 661, 1968.

4-14. Fjeldbo, G., Kliore, A.J., and Eshleman, V.R., Astron. J., Vol. 76, p. 381, 1971.

4-15. Howard, H.T., private communication, 1976.

and

4-16. von Roos, O.H., Yip, K.W., Escobal, P.R., Astronautica Acta, Vol. 18 (Supplement), p. 215, 1974.

4-17. Kliore, A.J., Levy, G.S., Cain, D.L., Fjeldbo, G., and Rasool, S.I., Science, Vol. 158, p. 1683, 1967.

4-18. Broadfoot, A.L., Kumar, S., Belton, M.J.S., and McElroy, M.B., Science, Vol. 183, p. 1315, 1974.

4-19. Kumar, S., and Hunten, D.M., J. Geophys. Res., Vol. 79, p. 2529, 1974.

4-20. Bauer, S.J., Hartle, R.E., and Herman, J.R., Nature, Vol. 225, p. 533, 1970.

4-21. Cloutier, P.A., and Daniell, R.E., Planetary Space Science, Vol. 21, p. 463, 1973.

4-22. Herman, J.R., Hartle, R.E., and Bauer, S.J., Planetary Space Science, Vol. 19, p. 443, 1971.

4-23. Michel, F.C., Rev. Geophys. Space Physics, Vol. 9, p. 427, 1971.

4-24. Spreiter, J.R., Summers, A.L., and Rizzi, A.W., Planetary Space Science, Vol. 18, p. 1281, 1970.

4-25. Wallis, M.K., Cosmic Electrodynamics, Vol. 3, p. 45, 1972.

4-26. Woo, R., Ishimaru, A., and Kendall, W.B., J. Atmos. Sci., Vol. 31, pp. 1698-1706, 1974.

4-27. Woo, R., J. Atmos. Sci., Vol. 32, No. 6., pp. 1084-1090, June 1975.

4-28. Dunne, J.A., Science, Vol. 185, pp. 141-142, 1974.

4-29. Fjeldbo, G., Kliore, A., Sweetnam, D., Esposito, P., Seidel, B., and Howard, T., accepted for publication in Icarus.

4-30. Fjeldbo, G., Seidel, B., Sweetnam, D., and Howard, T., J. Atmos. Sci., Vol. 32. pp. 1232-1236, 1975.

4-31. Fjeldbo, G., Kliore, A.J., and Eshleman, V.R., Astron. J., Vol. 76, pp. 123-140, 1971.

4-32. Murray, B.C., Belton, M.J.S., Danielson, G.E., Davies, M.E., Gault, D.E., Hapke, B., O'Leary, B., Strom, R.G., Suomi, V., and Trask, N., Science, Vol. 185, pp. 169-179, 1974.

4-33. Broadfoot, A.L., Kumar, S., Belton, M.J.S., and McElroy, M.B., Science, Vol. 185, pp. 166-169, 1974.

4-34. Hartle, R.E., Curtis, S.A., and Thomas G.E., J. Geophys. Res., Vol. 80, pp. 3689-3692, 1975.

4-35. Martin, W. L., "System Performance of the Dual-Channel Mu-II Sequential Ranging," in The Deep Space Network Progress Report 42-26, Jet Propulsion Laboratory, Pasadena, Calif., pp. 54-68, Apr. 15, 1975.

4-36. Woo, R., Yang, F.C., Yip, K.W., and Kendall, W.B., Ap. J., Vol. 210, pp. 568-574, Dec. 1, 1976.

4-37. Lotova, N.A., Soviet Phys. Uspekhi, Vol. 18, p. 292, 1975.

4-38. Tatarski, V.L., The Effects of the Turbulent Atmosphere on Wave Propagation, National Technical Information Service, Springfield, Va., 1971.

4-39. Woo, R., Yang, F.C., and Ishimaru, A., Ap. J., Vol. 210, pp. 593-602, 1976.

4-40. Cronyn, W.M., Ap. J., Vol. 174, p. 181, May 15, 1972.

4-41. Callahan, P.S., Ap. J., Vol. 199, p. 227, 1975.

4-42. Woo, R., Ap. J., Vol. 201, p. 238, 1975.

NASA—JPL—Coml., L.A., Calif

PUBLICATION 77-17